

1 **Prenatal conditions do not affect brain physiology and**
2 **learning in a lizard**

3 Pablo Recio^{1,‡}, Dalton C. Leibold¹, Ondi L. Crino^{1,2}, Christopher R. Friesen^{3,4}, Daniel W.A.
4 Noble¹

5 ¹ Division of Ecology and Evolution, Research School of Biology, The Australian National
6 University, Canberra, ACT 2601, Australia

7 ² Flinders University, College of Science and Engineering, Bedford Park, SA 5042, Australia

8 ³ University of Wollongong, Wollongong, NSW 2500, Australia

9 ⁴ Environmental Futures University of Wollongong, Wollongong, NSW 2500, Australia ‡

10 Corresponding author: pablo.reciosantiago@anu.edu.au

11 Pablo Recio ORCID: 0000-0002-5890-0218

12 Dalton C. Leibold ORCID: 0000-0001-9645-2033

13 Ondi L. Crino ORCID: 0000-0001-5700-1387

14 Christopher R. Friesen ORCID: 0000-0001-5338-7454

15 Daniel W.A. Noble ORCID: 0000-0001-9460-8743

16

17 **Abstract**

18 Early environmental factors like heat or stress hormones can impair learning through brain
19 metabolic function, crucial for neural development and synaptic plasticity. However, whether
20 early environments always result in cognitive impairment through changes in neural physiology
21 is not well-established outside of a few model systems. Here, we investigated the effects of
22 prenatal temperature and corticosterone (CORT) on brain mitochondrial activity and spatial
23 learning in the delicate skink (*Lampropholis delicata*). We treated eggs with either CORT or a
24 control vehicle and incubated at cold ($23 \pm 3^\circ\text{C}$) or hot ($28 \pm 3^\circ\text{C}$) temperatures. Juveniles were
25 tested in a spatial learning task over 40 days after which mitochondrial function in the medial
26 cortex was assessed. Despite among-individual variation in learning ability, mitochondrial
27 physiology and spatial learning in *L. delicata* remained robust to prenatal temperature and CORT
28 exposure. No significant relationship was found between mitochondrial function and cognitive
29 performance, contrary to predictions. Increased metabolic capacity correlated with higher ROS
30 production but did not affect oxidative damage, possibly due to protective mechanisms. These
31 findings highlight the physiological and cognitive resilience of *L. delicata* to early-life
32 challenges. Future research should explore whether this robustness extends to other brain
33 regions, cognitive domains, and life stages.

34 **Introduction**

35 Learning - the acquisition and consolidation of new information - enables animals to create new
36 associations between events, which can be essential for coping with environmental change
37 (Buchanan et al., 2013; Dukas, 2004; Leal and Powell, 2012). However, the capacity to form
38 new associations varies among individuals, potentially affecting their responses to environmental

39 challenges (Ward-Fear et al., 2016; Welklin et al., 2024). Learning faster may imply better
40 exploitation of resources or responding more efficiently to novel threats (Ward-Fear et al., 2016).
41 Consequently, individual differences in learning abilities can profoundly affect fitness, ultimately
42 influencing population growth rates and stability (Ward-Fear et al., 2016; Welklin et al., 2024).
43 Therefore, understanding the mechanisms that drive these differences is crucial for predicting
44 how populations will respond to novel conditions.

45 Factors like age, sex, or early-life conditions can have important effects on learning abilities
46 (Amiel and Shine, 2012; Amiel et al., 2014; Carazo et al., 2014; Lemaire et al., 2000; Noble et
47 al., 2014; Szuran et al., 1994; Zhu et al., 2004). Adverse developmental environments are
48 particularly influential, as the brain is highly sensitive to environmental inputs during early life
49 (Zhu et al., 2004). For example, early experiences can alter neurotransmitter production (Amani
50 et al., 2021), gene expression (Zhou et al., 2020), or brain structure (Amiel et al., 2017), with
51 lasting effects on cognition. Among the physiological mechanisms underlying learning,
52 mitochondrial activity is considered a key factor (Du et al., 2009; Picard and McEwen, 2014;
53 Picard et al., 2018; Siegel and Albers, 1994). The neural processes involved in learning impose
54 substantial energetic demands (Alexandrov and Pletnikov, 2022; Mann et al., 2021; McNay et
55 al., 2000), making efficient mitochondrial respiration essential (Du et al., 2009; Picard and
56 McEwen, 2014; Picard et al., 2018). Additionally, learning depends on a dense network of
57 functional neurons (Amiel et al., 2017; Lefebvre, 2011), which can be compromised by
58 excessive oxidative stress - a byproduct of mitochondrial metabolism (Du et al., 2009; Finkel and
59 Holbrook, 2000; Gong et al., 2011; Hoffmann and Spengler, 2018; Zhu et al., 2004). Studies on
60 mammals have shown the pervasive effects of mitochondrial physiology on cognitive abilities

61 (Cao et al., 2014; Hara et al., 2014; Zhu et al., 2004). However, the extent to which these effects
62 are generalisable to other taxa remains largely unexplored.

63 Since mitochondria are maternally inherited, maternal condition plays a fundamental role in
64 shaping offspring mitochondrial activity (Picard and McEwen, 2014). Maternal stress can also
65 influence how mitochondria operate in offspring (Zhu et al., 2004). Stressful situations
66 experienced by mothers can elevate glucocorticoids (GCs) (Sapolsky et al., 2000), which can
67 affect developing embryos (Uller et al., 2009) altering mitochondrial physiology through
68 transgenerational effects (Picard and McEwen, 2014). For instance, maternal stress has been
69 shown to contribute significantly to oxidative stress in the brain of rats (*Rattus norvegicus*) with
70 impacts on spatial learning abilities (Cao et al., 2014; Haussmann et al., 2012; Zhu et al., 2004).

71 Temperature is also a significant source of maternal stress in ectotherms. Thermal environments
72 outside the optimal range can elevate GCs in mothers, which can be passed to the offspring (see
73 Crino et al., 2023). Temperature can also directly influence offspring development, particularly
74 during early life (Crino et al., 2024; Noble et al., 2018). The prenatal thermal environment is
75 crucial in shaping mitochondrial function, affecting energy metabolism and oxidative stress
76 (Crino et al., 2024; Stier et al., 2022). Thus, the combined effects of prenatal GCs and
77 temperature may profoundly influence mitochondrial function, with important consequences for
78 brain development and cognition. However, the extent to which prenatal GCs and temperature
79 interact to shape cognitive abilities via mitochondrial physiology remains largely unknown
80 outside of a few model species (Cao et al., 2014; Haussmann et al., 2012; Zhu et al., 2004).

81 Here, we examined how prenatal temperature and corticosterone (CORT) — the primary GC in
82 reptiles — affect brain mitochondrial physiology and spatial learning in the delicate skink
83 (*Lampropholis delicata*). We hypothesized that prenatal CORT and temperature would influence

84 learning abilities by impacting brain mitochondrial activity. Specifically, we predicted that
85 prenatal CORT would decrease energy production while increasing oxidative damage (Costantini
86 et al., 2011; Gong et al., 2011; but see Crino et al., 2024), especially if CORT can alter cellular
87 components increasing ROS production without enhancing ATP synthesis or making them more
88 vulnerable to oxidative damage. Similarly, we predicted that high temperatures would decrease
89 mitochondrial efficiency (Crino et al., 2024; Závorka et al., 2021), but would reduce oxidative
90 stress (Treidel et al., 2016). We further predicted that the combined effects of CORT and
91 temperature would lead to complex interactions, with both factors negatively impacting
92 mitochondrial efficiency but having opposite effects on oxidative stress. These effects would
93 lead to differences in learning abilities, which could be affected by the balance between energy
94 production and oxidative stress (Alexandrov and Pletnikov, 2022; Du et al., 2009; Picard et al.,
95 2018). By examining these interactions, we aim to clarify how prenatal environmental factors
96 shape learning abilities through mitochondrial function, clarifying the mechanisms that mediate
97 the role of early-life conditions on cognitive development.

98 **Methods**

99 *Experimental animals*

100 Lizards came from a breeding colony established in the laboratory in 2019 from wild populations
101 in Sydney, Australia. The colony consisted of 270 adults in groups of two males and four
102 females. Eggs were collected from these groups between November 2023 to January 2024. After
103 collecting the eggs, we treated them with CORT or vehicle control and incubated them under two
104 different temperature regimes (see below). Clutch and egg identity were assigned immediately
105 after egg collection, and the eggs were incubated in individual cups until hatching. Hatchlings

106 were also kept in individual enclosures until the end of the experiment. For details on husbandry
107 and breeding conditions see *Methods 1: Animal husbandry in Supplementary Material*.

108 *Corticosterone and temperature manipulations*

109 We tested the combined effects of prenatal CORT and temperature by elevating CORT
110 concentrations in eggs and then incubating them under one of two temperature regimes (Cold -
111 23 ± 3 °C or Hot - 28 ± 3 °C). We used a partial split clutch design where eggs from a given
112 clutch were distributed equally across the four treatments when clutch sizes were larger than four
113 and randomly across treatments when less than four. CORT-treated eggs were topically supplied
114 with 5 µL of crystalline corticosterone (Sigma, Cat. No. C2505) dissolved in 100% ethanol at a
115 final concentration of 10 pg CORT/mL (CORT treatment), while Control eggs received an equal
116 volume of 100% Ethanol. CORT dose increased mean yolk CORT levels ~3.7x higher than
117 control eggs in previous studies ([Crino et al., 2024](#)). Eggs were then incubated in one of the two
118 previously mentioned temperature regimes that are within the natural limits of nest temperatures
119 in *L. delicata* ([Cheetham et al., 2011](#)).

120 *Spatial learning*

121 The spatial learning task involved training lizards to navigate a 6-arm maze to reach an exit
122 connected to a transport box that allowed us to return the lizards to their enclosure without
123 further contact. In each trial, lizards were placed by hand in the center of the maze and left to
124 acclimatise for two minutes. During acclimatisation, the central area was surrounded by a yellow
125 device mounted on a pulley system. At the start of each trial, this device was lifted to startle the
126 lizard. If the lizard did not immediately choose an arm, it was gently prodded with a brush at the
127 end of the tail. Once the lizard made a choice, the brush encouraged movement but without

128 guiding it towards any specific arm. If the lizard did not choose correctly after 20 errors — at
129 which point it typically ceased responding — the lizard was gently guided to the correct arm.

130 We assessed lizards' spatial learning using external cues for navigation while avoiding intra-
131 maze cues. Subtle intra-maze cues were avoided by replacing the maze every three trials with
132 one of four identical mazes. Each replacement preserved the correct arm's orientation and the
133 maze's position within the room, ensuring consistency for each individual. Additionally, the
134 maze was cleaned with 70% ethanol between trials to avoid the influence of chemical cues. The
135 correct arm was randomly assigned to one of the six arms for each trial to control for potential
136 side biases. We employed four maze orientations to counterbalance the number of lizards
137 assigned to each orientation across treatments.

138 The task was repeated once daily for 40 consecutive days, and the number of errors made by
139 each lizard was recorded. An error was defined as the lizard inserting its head into one of the
140 incorrect arms with each incorrect choice, including consecutive choices of the same arm,
141 counted as independent errors.

142 *Brain mitochondrial function*

143 Immediately after completing the tests, we quantified mitochondrial physiology in the brains of
144 lizards. We euthanized lizards via intraperitoneal injection of 10 mg/kg of a 10 mg/mL alfaxan
145 solution (a potent anesthetic), followed by decapitation. Before decapitation, we evaluated lizard
146 righting responses and the pinching reflexes in one of the front limbs.

147 We extracted the medial cortex in the telencephalon as this brain region is considered
148 homologous to the mammalian hippocampus, where spatial cognition is encoded (Naumann et
149 al., 2015; Rodríguez et al., 2002). The tissue was transferred to 1X PBS solution and then

150 homogenized mechanically using a 100 μ m mesh filter (pluriStrainer). The resultant homogenate
151 was divided into two aliquots: one was used fresh for measuring mitochondrial density,
152 membrane potential - a metric of mitochondrial metabolic capacity ([Martínez-Reyes et al., 2016](#))
153 - and superoxide (ROS) production; and the other was cryopreserved for later measurements of
154 DNA damage and lipid peroxidation.

155 Fresh homogenate suspensions were stained with 5 μ M MitoTracker Deep Red FM, 2.5 μ M
156 MitoTracker Orange CMTMRos, and 50 μ M MitoSOX Red. We used these fluorescent probes to
157 assess mitochondrial density, membrane potential, and ROS, respectively. We also added 5 μ L
158 of 10 μ g/mL Hoechst 33342 Nuclear Viability Dye to each sample to differentiate viable cells
159 from debris. These samples were analyzed in a flow cytometer within 2 hours of brain extraction.

160 The aliquots reserved for oxidative damage assays were stained with 10 μ g/mL Hoechst 33342
161 Nuclear Viability Dye and 100 μ M BODIPY 665/676 Lipid Peroxidation Sensor before
162 cryopreservation. These dyes were used to measure cell viability and lipid peroxidation,
163 respectively. The samples were then fixed in 1% Neutral-Buffered Formalin, washed, and
164 preserved in a 1X Tris-EDTA solution with 10% DMSO at -20 °C. On the day of the oxidative
165 damage assays, the samples were thawed, and DMSO was removed. Then, cell membranes were
166 permeabilized in 200 μ L of 1X PBS containing 20 μ M digitonin. Following permeabilization we
167 stained the samples with 20 μ L of 70 μ M 8-OHdG Polyclonal Antibody - a marker of DNA
168 damage - and allowed them to incubate overnight at 4 °C. The following day we counterstained
169 the cells with 20 μ L of 100 μ g/mL H+G Goat Anti-Rabbit Conjugate Antibody with Alexa-Fluor
170 488 and analyzed the samples using the flow cytometer. Oxidative damage assays were
171 performed within 6 months of the initial preparation of fresh samples.

172 Flow cytometry was performed on a 5-lasers flow cytometer (Becton Dickson LSRFortessa X-
173 20) using the default wavelength filters and a high-throughput plate reader. Detectors and voltage
174 settings for each assay were determined during pilot trials and remained consistent throughout
175 the experiment. Data was processed using FlowJo (v. 10.1) software. We obtained the mean
176 fluorescent intensity for mitochondrial density, metabolic capacity, ROS, DNA damage, and
177 lipid peroxidation. For further details on the homogenization, staining, or flow cytometry assays,
178 see *Methods 2: flow cytometry in Supplementary Material*. Sample sizes for DNA damage and
179 lipid peroxidation were smaller than for the other variables because of a plater reader
180 malfunction; however, data was missing randomly and we dealt with missing data in our
181 analyses (see below). We validated that our homogenates contained neurons in a pilot study that
182 used dyes specifically targeting neuronal nuclei (See *Brain validation in Supplementary*
183 *Material*). This pilot study also ensured that our gating strategy identified these neurons using
184 Flow cytometry.

185 *Statistical analyses*

186 We performed all analyses using the *brm* package (Bürkner, 2017), which fits Bayesian
187 multilevel models with *Stan* (Stan Development Team, 2024) with R version 4.4.0 (R Core
188 Team, 2021). We ran a series of univariate and multivariate models to test the effects of early
189 environment on each variable separately plus quantify the relationships between physiology and
190 learning. All models consisted of four MCMC chains of 8000 iterations, with a warmup interval
191 of 2000 iterations.

192 Univariate models were used to test the effects of early environment on each variable recorded:
193 mitochondrial density, metabolic capacity, ROS, DNA damage, lipid peroxidation, and the

194 number of errors as a measure of learning. In all the models, we included hormone treatment
195 (CORT vs Control), incubation temperature (Cold vs Hot), and their interaction. Sex and age
196 were included in preliminary models and excluded from the final models when they were not
197 significant. For all univariate models, clutch identity was included as a random factor.

198 Mitochondrial-related variables were log-transformed when necessary, and all were mean-
199 centered and standardized by dividing them by two times the standard deviation (Gelman, 2008).
200 These variables were considered to follow a normal distribution.

201 Learning was modeled as a function of trial, CORT, temperature, and their three-way interaction.
202 In this model, we included the trial within each level of lizard identity as a random slope. The
203 error structure was modelled using a negative binomial distribution with a logit link function
204 [negbinomial(link = "log")]. Otherwise, the procedure was as in the other models.

205 We used the posterior distributions of parameters from these models to test for differences
206 between treatments. Learning slopes were obtained using the 'trial' estimates and its interaction
207 with hormone and temperature treatments. Slope estimates less than 0 provide evidence of
208 learning. *pMCMC* was used to test the hypothesis that posterior distributions of slopes and slope
209 contrasts differed from zero. We considered an effect statistically significant when *pMCMC*
210 <0.05.

211 We fitted a multivariate structural equation model (SEM) using *brms* to explore direct and
212 indirect links between mitochondrial function and learning. The model was structured based on
213 theoretical expectations shown in Fig. 3. Any missing data was imputed during model fitting
214 using data augmentation (Noble and Nakagawa, 2021), but this was largely restricted to DNA
215 damage and lipid peroxidation. To obtain a measure of learning performance we extracted the
216 posterior distribution of individual learning slopes (i.e., changes in error over time) by including

217 a random trial slope for each lizard. Learning slopes and the rest of variables, were standardized
218 as before (see above). We assumed a Gaussian error distribution for all the variables in this
219 model. Factors found to be non-significant in the univariate models were excluded. Clutch
220 identity remained a random factor in our SEM model. Direct, indirect, and total effects were
221 derived from posterior estimates (Kline, 2005) (see Table S4).

222 Results

223 We started with 80 lizards - 20 per treatment - from 33 clutches. However, due to natural
224 mortality, only 79 lizards were included in the learning analyses, and 78 in the mitochondrial
225 analyses. We provide final sample sizes in all our figures.

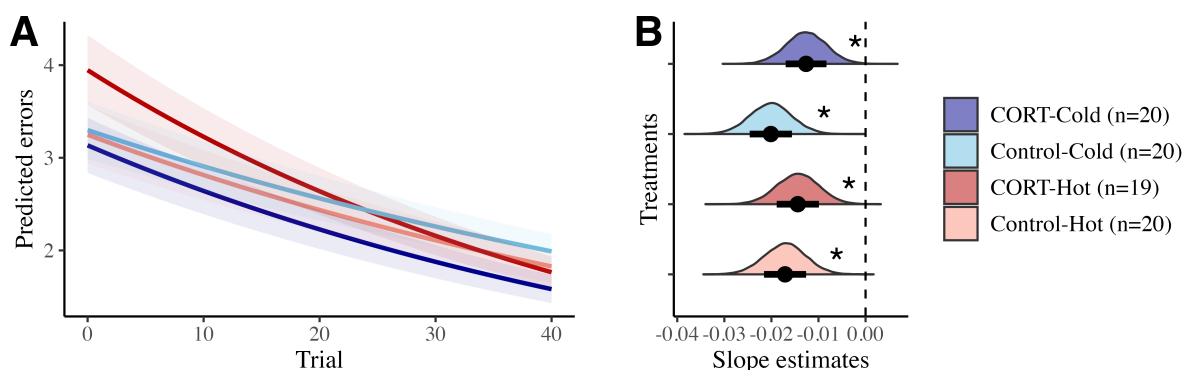


Fig. 1. Model estimates for learning analyses. (a) the predicted number of errors over trials. The lines represent the mean predicted number of errors for each trial, and the shaded areas indicate the standard error of the mean; both were obtained using the slope and intercept estimates from the posterior distributions. (b) shows the distribution of the estimates of slopes per each treatment. The x-axis represents the slope estimate, and in the y-axis are the density of the estimates. Points and bars represent the mean and standard error of the estimated slopes,

respectively. Dashed lines indicate value 0. The different colors in both panels indicate the different treatments. Asterisks in (b) indicate significant differences from 0.

226 We found that the lizards improved their choices over time, making less mistakes as the trials
227 progressed (see [Fig. 1](#) and Table S1). However, the learning rate was not influenced by CORT,
228 temperature, or their interaction (see contrasts in Table S2).

229 Mitochondrial density, metabolic capacity, ROS, DNA damage, and lipid peroxidation were also
230 not affected by prenatal conditions (see [Fig. 2](#) and Table S2). We did not find effects of sex and
231 age on mitochondrial physiology (see Table S3 and Tables S5-S9).

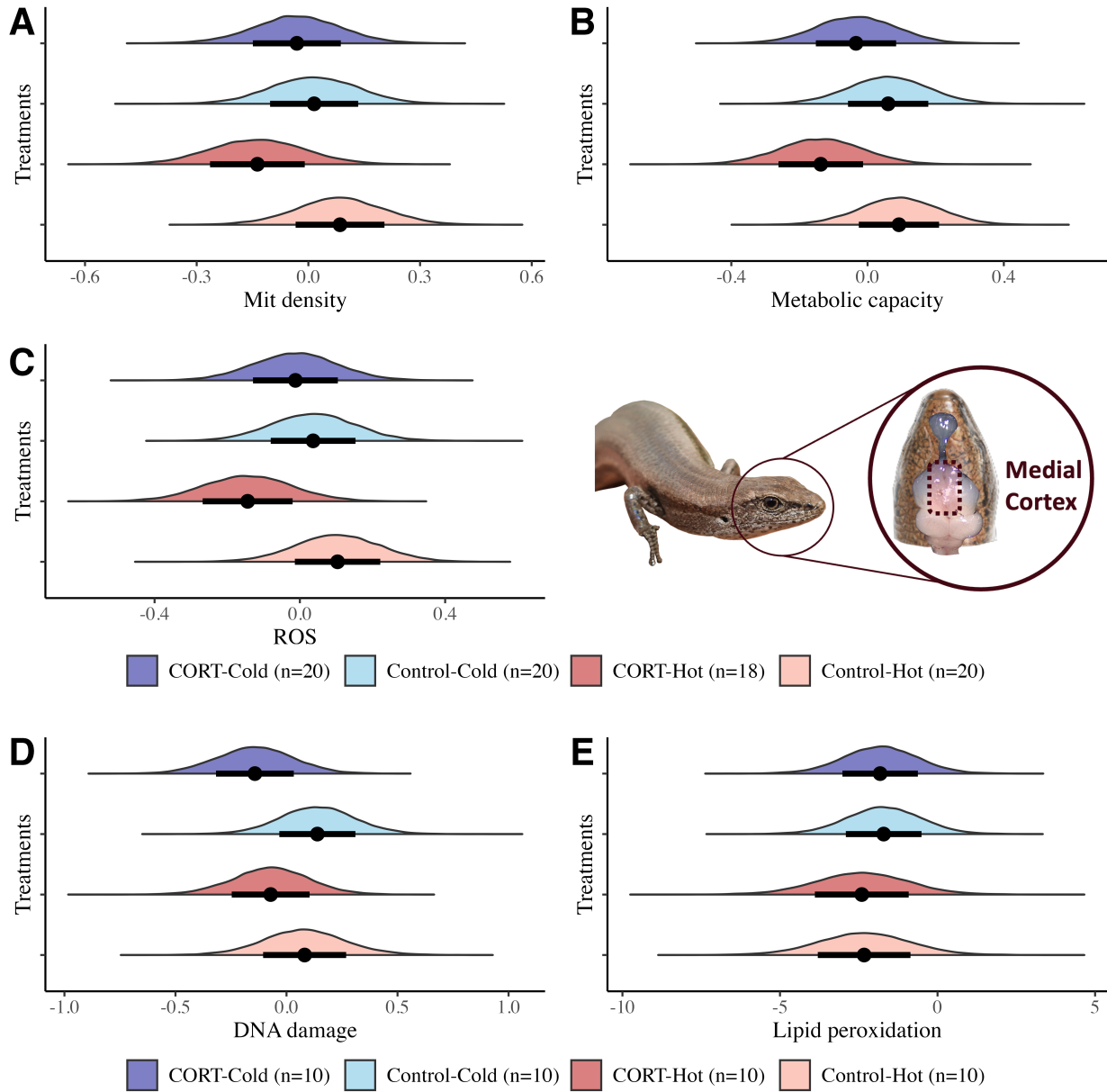


Fig. 2. Model estimates of mitochondrial density (a), metabolic capacity (b), ROS (c), DNA damage (d), and lipid peroxidation (e) in the medial cortex as a function of the different prenatal conditions. Note that for (d) and (e), these analyses do not account for missing data resulting from a flow cytometer malfunction that impacted one plate, so sample sizes are lower for univariate analyses. The x-axis represents the estimated values while the y-axis shows the

density of the estimates. Points and bars represent the mean and standard error of the estimated values, respectively. The different colors in both panels indicate the different treatments.

232 Our SEM showed that mitochondrial physiology was unrelated to learning abilities (see Fig. 3
 233 and Table S4). While we found that ROS production increased with metabolic capacity ($\beta =$
 234 1.090, 95% CI = [0.316, 1.862], $pMCMC < 0.05$), ROS was not related to oxidative damage (see
 235 Fig. 3 and Table S4).

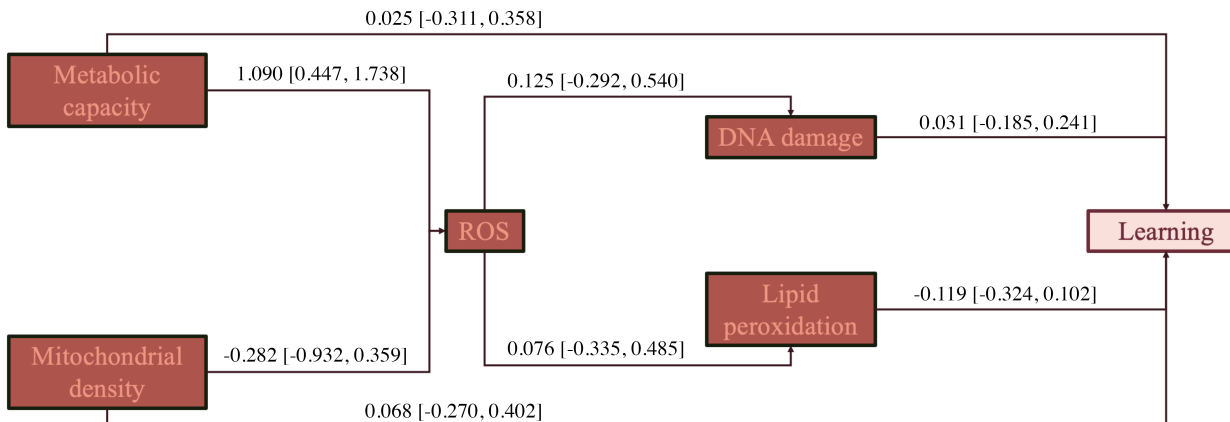


Fig. 3. Structural equation model testing hypothesized direct and indirect effects of physiology on learning. Arrows indicate the directionality of the estimate, and the values show the mean predicted coefficient and its 95% confidence interval.

236 Discussion

237 Lizards were able to learn a complex spatial task with marked improvements over time in their
 238 ability to choose the correct location. However, learning was neither influenced by prenatal
 239 conditions nor linked to mitochondrial function in the medial cortex, counter to what we

240 predicted. Despite ROS increasing with greater metabolic capacity as expected, this did not
241 result in a corresponding increase in oxidative damage in the medial cortex in *L. delicata*. We
242 discuss our results in relation to existing work exploring the underlying mechanisms of learning
243 and how early environments impact it below.

244 *Spatial learning is robust to prenatal conditions*

245 Lizards exhibited clear evidence for learning, but learning rates were not influenced by prenatal
246 CORT or temperature as we predicted, contrasting with findings in other taxa where incubation
247 temperature and prenatal GCs impacted learning and brain development ([Amiel and Shine, 2012](#);
248 [Amiel et al., 2017](#); [Dayananda and Webb, 2017](#); [Lemaire et al., 2000](#); [Zhu et al., 2004](#)). Our
249 results suggest that spatial learning abilities in *L. delicata* are buffered from adverse early
250 environmental conditions, consistent with our previous findings showing that behavioural
251 flexibility in this species is also unaffected by prenatal CORT or temperature ([Recio et al., 2025](#)).
252 *L. delicata*'s resilience may stem from the relevance of spatial cognition in lizards. For example,
253 spatial learning in velvet geckos (*Amalosia lesueuri*) enhances survival in the wild ([Dayananda
254 and Webb, 2017](#)). Future studies should investigate the mechanisms underlying this robustness
255 and the role of cognition in *L. delicata*'s fitness.

256 *Brain metabolic physiology is not affected by prenatal conditions*

257 Contrary to our predictions, prenatal temperature and CORT did not significantly influence
258 mitochondrial physiology in the medial cortex of *L. delicata*. Studies in other taxa have shown
259 that incubation at high temperatures decreases energy production and oxidative stress ([Treidel et
260 al., 2016](#); [Závorka et al., 2021](#)), while elevated GCs or maternal stress is related to lower
261 mitochondrial efficiency and higher oxidative damage ([Costantini et al., 2011](#); [Gong et al., 2011](#);

262 but see [Crino et al., 2024](#)). In *L. delicata*, high incubation temperatures are known to decrease
263 mitochondrial efficiency in the liver ([Crino et al., 2024](#)). However, our study shows that
264 mitochondrial physiology in *L. delicata*'s brain is robust to both incubation temperature and
265 prenatal CORT. Differences between liver and brain could reflect tissue-dependent responses to
266 early-life conditions, highlighting the importance of studying these effects across multiple tissues
267 ([Casagrande et al., 2023](#)).

268 *Variation in brain metabolic physiology is not related to learning abilities*
269 Mitochondria play a critical role in cognitive function by synthesizing energy ([Du et al., 2009](#);
270 [Picard and McEwen, 2014](#); [Picard et al., 2018](#); [Siegel and Albers, 1994](#)), and by affecting the
271 rate of cell senescence and death caused by oxidative damage ([Alexandrov and Pletnikov, 2022](#);
272 [Mann et al., 2021](#); [McNay et al., 2000](#)). Our findings contrast with past studies and suggest that
273 energy limitations do not impact spatial learning in *L. delicata*. The lack of association between
274 mitochondrial density, mitochondrial capacity, and learning abilities may result from lizards
275 being able to maintain energy production above the threshold required to prevent cognitive
276 dysfunction. The generally low energetic demands of ectothermic organisms compared to
277 endotherms may make this possible and explain why we found no effect when they seem
278 common in mammals ([Cao et al., 2014](#); [Hara et al., 2014](#)). Alternatively, individuals with higher
279 respiration and ROS may be upregulating antioxidant production ([Rice et al., 2002](#)).
280 Interestingly, despite finding a significant positive relationship between metabolic capacity and
281 ROS in the medial cortex, the heightened ROS production did not lead to greater oxidative
282 damage. The strong relationship between ROS and mitochondrial capacity aligns with the role of
283 mitochondrial membrane potential in driving ATP synthesis and electron transport, processes

284 that inherently generate ROS as byproducts (Rice et al., 2002). Normally, moderate ROS levels
285 serve essential signaling functions and are controlled by antioxidants (Rice et al., 2002; Terman
286 and Brunk, 2006). However, excessive ROS production can exceed antioxidant action, leading to
287 oxidative stress and cellular dysfunction (Rice et al., 2002; Terman and Brunk, 2006). The lack
288 of oxidative damage from increased ROS strongly suggests that antioxidants could deal with
289 these levels of ROS. As such, DNA damage and lipid peroxidation in the medial cortex were not
290 linked to spatial learning in *L. delicata* possibly because neurons were effectively buffered from
291 damaging free radicals. Nevertheless, since oxidative damage can accumulate over time (Terman
292 and Brunk, 2006), the relationships between oxidative damage and cognitive dysfunction could
293 become more pronounced in older individuals (Hara et al., 2014). Future research should
294 investigate the long-term consequences of mitochondrial activity on brain health and the
295 potential mechanisms that sustain cognitive resilience in *L. delicata*.

296 *Conclusions*

297 We found that spatial learning in *L. delicata* was not influenced by prenatal CORT or
298 temperature, nor was mitochondrial physiology in the medial cortex. Additionally, there was no
299 relationship between mitochondrial function and learning abilities in a spatial task. However, we
300 found that ROS production increased with metabolic capacity, suggesting that links between
301 mitochondrial respiration and oxidative stress may become more pronounced under higher
302 energetic demands or with aging, potentially influencing cognitive function over time.

303 **Ethics**

304 Both the breeding animals and the experimental lizards were provided humane laboratory
305 housing, with thermoregulatory opportunities, light (UV and heat) and moderate humidity levels

306 (see Methods 1: Animal husbandry in Supplementary Material for details). Euthanasia was
307 performed by intraperitoneal injection of 10 mg/kg of a 10 mg/mL alfaxan solution (a potent
308 anesthetic) followed by decapitation. We monitored the animals to ensure no irritation from the
309 agent as indicated by distressed animals. Before disposing of the lizard, we confirmed the
310 absence of righting response and the pinching reflex in one of the front limbs. All the protocols
311 complied with Australian law and were approved by the Australian National University Animal
312 Experimentation Ethics Committee (A2022_33).

313 **Data accessibility**

314 All data, data description, and R code are available in public repository <https://github.com/Pablo->
315 [Recio/CORT-Temp_Spatial_learning](https://github.com/Pablo-Recio/CORT-Temp_Spatial_learning).

316 **Declaration of AI use**

317 We declare Chat GPT-4 was used for questions related to code checking when there were
318 unknown errors, but we did not rely on AI for the creation of any of the content in the
319 manuscript, which was written fully by the authors. Last time Chat GPT-4 was used was
320 February 2025.

321 **Authors' contributions**

322 P.R.: conceptualization, methodology, data collection, data curation, formal analysis, writing—
323 original draft, writing—review and editing; D.C.L.: conceptualization, methodology, data
324 collection, writing—review and editing; O.C.: conceptualization, methodology, writing—review
325 and editing; C.F.: conceptualization, methodology, funding acquisition, writing—review and
326 editing; D.N.: conceptualization, methodology, funding acquisition, project administration,

327 resources, supervision, writing—review and editing.
328 All authors gave final approval for publication and agreed to be held accountable for the work
329 performed therein.

330 **Conflict of interest declaration**

331 We declare we have no competing interests.

332 **Funding**

333 This work was supported by a National Australian University fellowship (to P.R. and D.C.L.),
334 and the Australian Research Council (grant no. DP210101152) to D.N. and C.R.F.

335 **Acknowledgements**

336 We thank Mick Devoy and the Cytometry, Histology and Spatial Multiomics team for their
337 advice and help throughout the flow cytometry protocols. We thank the help and assistance of our
338 lab technicians Benjamin Durant and Michelle Stephens for taking care of the lizards. We also
339 thank ANU MakerSpace, where we designed and built the prototypes of the 3D printed feeders.
340 The authors acknowledge Microscopy Australia (ROR: 042mm0k03) at the Centre for Advanced
341 Microscopy, The Australian National University, a facility enabled by NCRIS and university
342 support. We specifically thank Dr Angus Rae and Dr Daryl Webb for their help with microscopy
343 protocols. Finally, we wish to acknowledge the anonymous reviewers for their valuable feedback
344 on the manuscript.

345 **References**

346 **Alexandrov, Y. I. and Pletnikov, M. V. (2022). Neuronal metabolism in learning and memory:**
347 **The anticipatory activity perspective. *Neuroscience & Biobehavioral Reviews* 137, 104664.**

- 348 **Amani, M., Houwing, D. J., Homberg, J. R. and Salari, A.-A.** (2021). Perinatal fluoxetine
349 dose-dependently affects prenatal stress-induced neurobehavioural abnormalities, HPA-axis
350 functioning and underlying brain alterations in rat dams and their offspring. *Reproductive*
351 *Toxicology* **104**, 27–43.
- 352 **Amiel, J. J. and Shine, R.** (2012). Hotter nests produce smarter young lizards. *Biology Letters*
353 **8**, 372–374.
- 354 **Amiel, J. J., Lindström, T. and Shine, R.** (2014). Egg incubation effects generate positive
355 correlations between size, speed and learning ability in young lizards. *Animal Cognition* **17**, 337–
356 347.
- 357 **Amiel, J. J., Bao, S. and Shine, R.** (2017). The effects of incubation temperature on the
358 development of the cortical forebrain in a lizard. *Animal Cognition* **20**, 117–125.
- 359 **Buchanan, K. L., Grindstaff, J. L. and Pravosudov, V. V.** (2013). Condition dependence,
360 developmental plasticity, and cognition: Implications for ecology and evolution. *Trends in*
361 *Ecology & Evolution* **28**, 290–296.
- 362 **Bürkner, P.-C.** (2017). Brms: An r package for bayesian multilevel models using stan. *Journal*
363 *of statistical software* **80**, 1–28.
- 364 **Cao, K., Zheng, A., Xu, J., Li, H., Liu, J., Peng, Y., Long, J., Zou, X., Li, Y., Chen, C., et al.**
365 (2014). AMPK activation prevents prenatal stress-induced cognitive impairment: Modulation of
366 mitochondrial content and oxidative stress. *Free Radical Biology and Medicine* **75**, 156–166.
- 367 **Carazo, P., Noble, D. W. A., Chandrasoma, D. and Whiting, M. J.** (2014). Sex and boldness
368 explain individual differences in spatial learning in a lizard. *Proceedings of the Royal Society B:*
369 *Biological Sciences* **281**, 20133275.
- 370 **Casagrande, S., Dzialo, M., Trost, L., Malkoc, K., Sadowska, E. T., Hau, M., Pierce, B.,**
371 **McWilliams, S. and Bauchinger, U.** (2023). Mitochondrial metabolism in blood more reliably
372 predicts whole-animal energy needs compared to other tissues. *Iscience* **26**.
- 373 **Cheetham, E., Doody, J. S., Stewart, B. and Harlow, P.** (2011). Embryonic mortality as a cost
374 of communal nesting in the delicate skink. *Journal of Zoology* **283**, 234–242.
- 375 **Costantini, D., Marasco, V. and Møller, A. P.** (2011). A meta-analysis of glucocorticoids as
376 modulators of oxidative stress in vertebrates. *Journal of Comparative Physiology B* **181**, 447–
377 456.
- 378 **Crino, O. L., Bonduriansky, R., Martin, L. B. and Noble, D. W. A.** (2023). A conceptual
379 framework for understanding stressinduced physiological and transgenerational effects on
380 population responses to climate change. *Evolution Letters*.
- 381 **Crino, O. L., Wild, K. H., Friesen, C. R., Leibold, D., Laven, N., Peardon, A. Y., Recio, P.,**
382 **Salin, K. and Noble, D. W.** (2024). From eggs to adulthood: Sustained effects of early
383 developmental temperature and corticosterone exposure on physiology and body size in an
384 australian lizard. *Journal of Experimental Biology* **227**.

- 385 **Dayananda, B. and Webb, J. K.** (2017). Incubation under climate warming affects learning
386 ability and survival in hatchling lizards. *Biology Letters* **13**, 20170002.
- 387 **Du, J., Wang, Y., Hunter, R., Wei, Y., Blumenthal, R., Falke, C., Khairova, R., Zhou, R.,**
- 388 Yuan, P., Machado-Vieira, R., et al.
- 389 (2009). Dynamic regulation of mitochondrial function by glucocorticoids. *Proceedings of the National Academy of Sciences* **106**, 3543–3548.
- 390 **Dukas, R.** (2004). Evolutionary Biology of Animal Cognition. *Annual Review of Ecology, Evolution, and Systematics* **35**, 347–374.
- 392 **Finkel, T. and Holbrook, N. J.** (2000). Oxidants, oxidative stress and the biology of ageing. *Nature* **408**, 239–247.
- 394 **Gelman, A.** (2008). Scaling regression inputs by dividing by two standard deviations. *Statistics in medicine* **27**, 2865–2873.
- 396 **Gong, Y., Chai, Y., Ding, J.-H., Sun, X.-L. and Hu, G.** (2011). Chronic mild stress damages mitochondrial ultrastructure and function in mouse brain. *Neuroscience Letters* **488**, 76–80.
- 398 **Hara, Y., Yuk, F., Puri, R., Janssen, W. G. M., Rapp, P. R. and Morrison, J. H.** (2014). Presynaptic mitochondrial morphology in monkey prefrontal cortex correlates with working memory and is improved with estrogen treatment. *Proceedings of the National Academy of Sciences* **111**, 486–491.
- 402 **Haussmann, M. F., Longenecker, A. S., Marchetto, N. M., Juliano, S. A. and Bowden, R. M.** (2012). Embryonic exposure to corticosterone modifies the juvenile stress response, oxidative stress and telomere length. *Proceedings of the Royal Society B: Biological Sciences* **279**, 1447–1456.
- 406 **Hoffmann, A. and Spengler, D.** (2018). The Mitochondrion as Potential Interface in Early-Life Stress Brain Programming. *Frontiers in Behavioral Neuroscience* **12**, 306.
- 408 **Kline, R. B.** (2005). Principles and practice of structural equation modeling 2nd ed. *New York: Guilford* 3.,
- 410 **Leal, M. and Powell, B. J.** (2012). Behavioural flexibility and problem-solving in a tropical lizard. *Biology Letters* **8**, 28–30.
- 412 **Lefebvre, L.** (2011). Taxonomic counts of cognition in the wild. *Biology Letters* **7**, 631–633.
- 413 **Lemaire, V., Koehl, M., Le Moal, M. and Abrous, D. N.** (2000). Prenatal stress produces learning deficits associated with an inhibition of neurogenesis in the hippocampus. *Proceedings of the National Academy of Sciences* **97**, 11032–11037.
- 416 **Mann, K., Deny, S., Ganguli, S. and Clandinin, T. R.** (2021). Coupling of activity, metabolism and behaviour across the *Drosophila* brain. *Nature* **593**, 244–248.
- 418 **Martínez-Reyes, I., Diebold, L. P., Kong, H., Schieber, M., Huang, H., Hensley, C. T., Mehta, M. M., Wang, T., Santos, J. H., Woychik, R., et al.** (2016). TCA cycle and

- 420 mitochondrial membrane potential are necessary for diverse biological functions. *Molecular cell*
421 **61**, 199–209.
- 422 **McNay, E. C., Fries, T. M. and Gold, P. E.** (2000). [Decreases in rat extracellular hippocampal](#)
423 [glucose concentration associated with cognitive demand during a spatial task](#). *Proceedings of the*
424 *National Academy of Sciences* **97**, 2881–2885.
- 425 **Naumann, R. K., Ondracek, J. M., Reiter, S., Shein-Idelson, M., Tosches, M. A.,**
426 **Yamawaki, T. M. and Laurent, G.** (2015). The reptilian brain. *Current Biology* **25**, R317–
427 R321.
- 428 **Noble, D. W. and Nakagawa, S.** (2021). Planned missing data designs and methods: Options for
429 strengthening inference, increasing research efficiency and improving animal welfare in
430 ecological and evolutionary research. *Evolutionary applications* **14**, 1958–1968.
- 431 **Noble, D. W. A., Byrne, R. W. and Whiting, M. J.** (2014). [Age-dependent social learning in a](#)
432 [lizard](#). *Biology Letters* **10**, 20140430.
- 433 **Noble, D. W. A., Stenhouse, V. and Schwanz, L. E.** (2018). [Developmental temperatures and](#)
434 [phenotypic plasticity in reptiles: A systematic review and meta-analysis: Incubation temperature](#)
435 [and plasticity](#). *Biological Reviews* **93**, 72–97.
- 436 **Picard, M. and McEwen, B. S.** (2014). [Mitochondria impact brain function and cognition](#).
437 *Proceedings of the National Academy of Sciences* **111**, 7–8.
- 438 **Picard, M., McEwen, B. S., Epel, E. S. and Sandi, C.** (2018). [An energetic view of stress:](#)
439 [Focus on mitochondria](#). *Frontiers in Neuroendocrinology* **49**, 72–85.
- 440 **R Core Team** (2021). [R: A language and environment for statistical computing](#).
- 441 **Recio, P., Leibold, D. C., Crino, O. L., Wild, K. H., Friesen, C. R., Mauclaire, B., Peardon,**
442 **A. Y. and Noble, D. W.** (2025). Early environmental conditions do not impact behavioural
443 flexibility in an invasive and noninvasive lizard species. *Animal Behaviour* 123106.
- 444 **Rice, M., Forman, R., Chen, B., Avshalumov, M., Cragg, S. and Drew, K.** (2002). Brain
445 antioxidant regulation in mammals and anoxia-tolerant reptiles: Balanced for neuroprotection
446 and neuromodulation. *Comparative Biochemistry and Physiology Part C: Toxicology &*
447 *Pharmacology* **133**, 515–525.
- 448 **Rodríguez, F., López, J. C., Vargas, J. P., Gómez, Y., Broglio, C. and Salas, C.** (2002).
449 Conservation of spatial memory function in the pallial forebrain of reptiles and ray-finned fishes.
450 *Journal of Neuroscience* **22**, 2894–2903.
- 451 **Sapolsky, R. M., Romero, L. M. and Munck, A. U.** (2000). How Do Glucocorticoids Influence
452 Stress Responses? Integrating Permissive, Suppressive, Stimulatory, and Preparative Actions.
453 **21**,
- 454 **Siegel, G. J. and Albers, R. W.** (1994). *Basic neurochemistry: Molecular, cellular, and medical*
455 *aspects*. Raven Press.

- 456 **Stan Development Team** (2024). *RStan: The R interface to Stan*.
- 457 **Stier, A., Monaghan, P. and Metcalfe, N. B.** (2022). Experimental demonstration of prenatal
458 programming of mitochondrial aerobic metabolism lasting until adulthood. *Proceedings of the
459 Royal Society B* **289**, 20212679.
- 460 **Szuran, T., Zimmermann, E. and Welzl, H.** (1994). Water maze performance and
461 hippocampal weight of prenatally stressed rats. *Behavioural Brain Research* **65**, 153–155.
- 462 **Terman, A. and Brunk, U. T.** (2006). Oxidative stress, accumulation of biological ‘garbage’,
463 and aging. *Antioxidants & redox signaling* **8**, 197–204.
- 464 **Treidel, L., Carter, A. and Bowden, R.** (2016). Temperature experienced during incubation
465 affects antioxidant capacity but not oxidative damage in hatchling red-eared slider turtles
466 (*trachemys scripta elegans*). *Journal of Experimental Biology* **219**, 561–570.
- 467 **Uller, T., Hollander, J., Astheimer, L. and Olsson, M.** (2009). Sex-specific developmental
468 plasticity in response to yolk corticosterone in an oviparous lizard. *Journal of Experimental
469 Biology* **212**, 1087–1091.
- 470 **Ward-Fear, G., Pearson, D., Brown, G., Rangers, B. and Shine, R.** (2016). Ecological
471 immunization: In situ training of free-ranging predatory lizards reduces their vulnerability to
472 invasive toxic prey. *Biology letters* **12**, 20150863.
- 473 **Welklin, J. F., Sonnenberg, B. R., Branch, C. L., Heinen, V. K., Pitera, A. M., Benedict, L.
474 M., Whitenack, L. E., Bridge, E. S. and Pravosudov, V. V.** (2024). Spatial cognitive ability is
475 associated with longevity in food-caching chickadees. *Science* **385**, 1111–1115.
- 476 **Závorka, L., Crespel, A., Dawson, N. J., Papatheodoulou, M., Killen, S. S. and Kainz, M. J.**
477 (2021). Climate change-induced deprivation of dietary essential fatty acids can reduce growth
478 and mitochondrial efficiency of wild juvenile salmon. *Functional Ecology* **35**, 1960–1971.
- 479 **Zhou, Q., Suzuki, A., Iinuma, M., Wang, K.-Y., Kubo, K. and Azuma, K.** (2020). Effects of
480 maternal chewing on prenatal stress-induced cognitive impairments in the offspring via multiple
481 molecular pathways. *International Journal of Molecular Sciences* **21**, 5627.
- 482 **Zhu, Z., Li, X., Chen, W., Zhao, Y., Li, H., Qing, C., Jia, N., Bai, Z. and Liu, J.** (2004).
483 Prenatal stress causes gender-dependent neuronal loss and oxidative stress in rat hippocampus.
484 *Journal of Neuroscience Research* **78**, 837–844.
- 485

486 **Supplementary Material**

487 *Methods 1: Animal husbandry*

488 *Breeding colony* - Juveniles of *L. delicata* came from a breeding colony established in the
489 laboratory since 2019. This colony consisted of 270 adults housed in plastic containers (41.5 L x
490 30.5 W x 21 H cm) with six lizards (two males and four females) per enclosure. Enclosures were
491 provided with shelter, nonstick matting, and several small water dishes. The lizards were fed
492 approx. 40 mid-size crickets (*Acheta domestica*) per enclosure three days a week, and water was
493 given daily. The crickets were dusted with calcium weekly and multivitamin and calcium
494 biweekly. Room temperatures were set to 22-24 °C, but we also provided the enclosures with a
495 heat chord and a heat lamp following a 12 h light:12 h dark cycle keeping warm side of
496 enclosures is usually at 34 °C.

497 *Eggs collection and incubation* - Between mid-November 2023 to mid-January 2024, we placed
498 a small box (12.5 L x 8.3 W x 5 H cm) with moist vermiculite in one side of the communal
499 enclosures to provide females with a place to lay the eggs. These boxes were checked three days
500 a week. After egg collection, we measured length and width with a digital caliper to the nearest
501 0.1 mm and weighted the eggs with a digital scale ± 0.001g error. Then eggs were treated with
502 CORT or vehicle (see CORT and temperature manipulation below) and were placed in
503 individual cups (80 mL) with moist vermiculite (12 parts water to 4 parts vermiculite). The cups
504 were covered with cling wrap to retain moisture and left in two incubators at two different
505 temperatures (see CORT and temperature manipulation below) until hatching.

506 *Hatchlings* - Incubators were checked three times a week for hatchlings. Lizards were measured
507 and weighed immediately after hatching. snout-vent length (SVL) and tail length (TL) were

508 measured to the nearest millimeter, and weight was recorded using a digital scale with an
509 accuracy of ± 0.001 g. Hatchlings were then placed in individual enclosures (18.7L x 13.2W x
510 6.3H cm) with nonstick matting and a small water dish. Watering, feeding, and temperature
511 conditions were maintained as for adults (see above).

512

513 *Methods 2: flow cytometry*

514 *Brain mitochondrial activity*

515 **Homogenates:** After the medial cortex was extracted, it was transferred immediately to 1.5mL
516 centrifuge tubes containing 100 μ L of cold 1X PBS and kept on ice until further processing. The
517 tissue was mechanically homogenized by placing the tissue in the well of a 100 μ m mesh filter
518 (pluriStrainer) affixed atop a 1.5mL centrifuge tube, then mashed with the rubber end of an
519 insulin syringe stopper. The resulting homogenate was then rinsed through the filter with
520 1000 μ L of cold 1X PBS to prepare a homogenate suspension. Following homogenization, we
521 centrifuged each sample at 1000 RCF for 10 minutes to pellet cells, then removed the
522 supernatant (hereafter, this process referred to as ‘washing’) and resuspended the cells in 500 μ L
523 1x PBS. This step was performed to remove cellular debris from homogenates.

524 From each 500 μ L suspension of homogenate collected on a given trial day, we first added 100 μ L
525 of homogenate to a pooled sample of each tissue type to use for single-color controls, and the
526 remaining 400 μ L of homogenate was split among two 200 μ L aliquots. One aliquot was used
527 fresh to measure mitochondrial function (mitochondrial density, membrane potential, ROS), one
528 aliquot was cryopreserved for later measurements of oxidative damage (8-OHdG, lipid
529 peroxidation), and the third aliquot was cryopreserved for a different experiment.

530 **Staining fresh samples:** From fresh homogenate suspensions, we loaded the wells of a 96-well
531 flat-bottom plate (Nunclon) with 50 μ L of homogenate in duplicates (2 wells per homogenate).
532 To each replicate well, we added 5 μ L of a fluorescent probe mix containing equal parts 5 μ M
533 MitoTracker Deep Red FM, 2.5 μ M MitoTracker Orange CMTMRos, and 50 μ M MitoSOX Red.
534 We used these fluorescent probes as indicators of mitochondrial density, mitochondrial

535 membrane potential, and superoxide (ROS) production, respectively. We then added 5 μ L of 10
536 μ g/mL Hoechst 33342 Nuclear Viability Dye to each sample, which we used to distinguish live,
537 viable, intact cells from cellular debris. We then loaded 6 wells with 50 μ L of homogenate taken
538 from each pooled homogenate suspension (12 wells total), which were to be negative and single-
539 color controls. One well was left unstained as a negative control, one was stained with all the
540 probes to be a positive control, and the remaining four wells were treated with 5 μ L of one of
541 5 μ M MitoTracker Deep Red FM, 2.5 μ M MitoTracker Orange CMTMRos, 50 μ M MitoSOX
542 Red, or 10 μ g/mL Hoechst 33342 Nuclear Viability Dye. Any remaining pooled homogenate
543 was fixed and frozen as previously described. We incubated the loaded plate at 32 °C for 30
544 minutes to stain and then diluted the samples with 50 μ L cold 1x PBS to halt the staining process.
545 Upon the completion of staining, samples were immediately transferred to flow cytometry
546 facilities for data collection and were sampled within 2 hours. Samples prepared this way
547 remained viable for flow cytometry for approximately 5 hours post-staining at room temperature
548 (~19°C) before cells began rapidly degrading (DCL, personal observation).

549 The aliquots destined to the analysis of oxidative damage were stained with 20 μ L (10 μ L for
550 controls) of 10 μ g/mL Hoechst 33342 Nuclear Viability Dye and 20 μ L of 100 μ M BODIPY
551 665/676 Lipid Peroxidation Sensor and incubated at 32°C for 20 minutes. Following staining, we
552 washed cells to prevent further binding of unbound fluorescent probes, then resuspended the
553 pellet and continue with cryopreservation.

554 **Cryopreservation:** Aliquots were fixed first by adding the samples into a 1mL solution of 1%
555 Neutral-Buffered Formalin (as a fixative agent) and incubating them at 32°C for 20 min. Then
556 washed the samples and resuspended the cells in 1mL cold 1X Tris-EDTA (chelates metals that

557 can damage DNA during freezing) and 10% DMSO (a cryoprotectant). Samples were stored at -
558 20°C until oxidative damage assays.

559 **Staining cryopreserved samples:** Assays of oxidative damage from cryopreserved samples
560 were performed within 6 months of the initial processing and analysis of fresh samples. On the
561 day of oxidative damage assays, we rapidly thawed frozen samples by briefly (1-2 minutes)
562 submerging them in hot water. We washed each thawed sample twice, the first time resuspending
563 the pelleted cells in 1000µL warm 1X Tris-EDTA, and the second time in 200µL warm 1X PBS
564 containing 20µM digitonin. We incubated the samples at 32°C for 20 minutes to permeabilize
565 the cell membrane, after which we washed the homogenate and resuspended the pelleted cells in
566 200µL 1X PBS. We added 20µL of 70µM 8-OHdG Polyclonal Antibody to each sample, and we
567 left the homogenate overnight (~12 hours) for the antibody to bind to 8-OHdG, a marker of
568 oxidative damage on DNA. The following day we counterstained the cells with 20µL of 100
569 µg/mL H+G Goat Anti-Rabbit Conjugate Antibody with Alexa-Fluor 488 at 32°C for 20
570 minutes. After the cells had been tagged with 8-OHdG antibodies and counterstained, we washed
571 the cells once more and resuspended the pellet in 400µL of 1X PBS. Unstained and single-color
572 controls were treated identically to samples, but stained with only up to one of BODIPY
573 665/676, Hoechst 33342, 8-OHdG antibody, or Alexa-Fluor 488 conjugate. Additionally, one
574 control was stained with both 8-OHdG antibody and the Alexa-Fluor 488 conjugate. We then
575 loaded a 96-well plate with 100µL of each single-color control and 100µL in triplicate of each
576 sample. We performed all flow cytometry assays on samples within 48-hours of thawing the
577 samples.

578 **Flow cytometry:** All flow cytometry assays were performed using a flow cytometer with 5-
579 lasers (blue, red, yellow-green, violet, and ultraviolet), 20 detectors, and a high-throughput plate

580 reader (Becton Dickson LSRFortessa X-20) using the default wavelength filters on detectors.

581 Immediately prior to all assays, we performed a quality-control check and laser alignment using

582 the CS&T function of BD FACSDiva (v. 8.0.1) and BD CS&T fluorescent beads (Lot

583 No. 30664) diluted at 1 drop to 150 μ L 1X PBS. During data collection, data for single-color

584 controls was filtered using a liberal threshold of 200 on the FSC (roughly, cell size) detector,

585 while data from samples was filtered using a threshold of 200 on the BUV-496 (Hoechst 33342)

586 detector. These thresholds were chosen to filter small debris or inviable or non-intact cells from

587 our observations. The detectors and voltage settings used in data acquisition for each assay type

588 (mitochondrial function, oxidative damage) were determined during pilot trials prior to assays

589 and were not changed during assays to allow for comparison among different plates and samples

590 throughout the experiment. Voltages were chosen to center the distribution of observations in

591 each channel at 10³ fluorescent intensity and reduce observations of off-scale (<10¹ or >10⁵)

592 events. For the mitochondrial function assay, we recorded data from the following channels (in

593 brackets: voltage; parameter): FSC (44; forward scatter), SSC (180; side scatter), Alexa-Fluor

594 488 (544; autofluorescence), BUV-496 (450; Hoechst 33342), APC (647; MitoTracker Deep Red

595 FM), PE (522; MitoTracker Orange CMTMRos), and PerCP-Cy5-5 (592; MitoSOX Red)

596 channels. For the oxidative damage assay, we recorded data from the following channels: FSC

597 (425; forward scatter), SSC (300; side scatter), Alexa-Fluor 488 (275; 8-OHdG Antibody +

598 Alexa-Fluor 488 conjugate), BUV-496 (525; Hoechst 33342), and PE-Cy5 (850; BODIPY

599 665/676). Fluorescent intensity data was collected via the BD FACSDiva (v. 8.0.1) software,

600 with no compensation applied during data collection, and all on a linear scale (detectable range

601 of 0-252166). We recorded data for both the area and height of the fluorescent signal, but only

602 used the area in downstream analyses, with height being recorded for the sake of quality control.

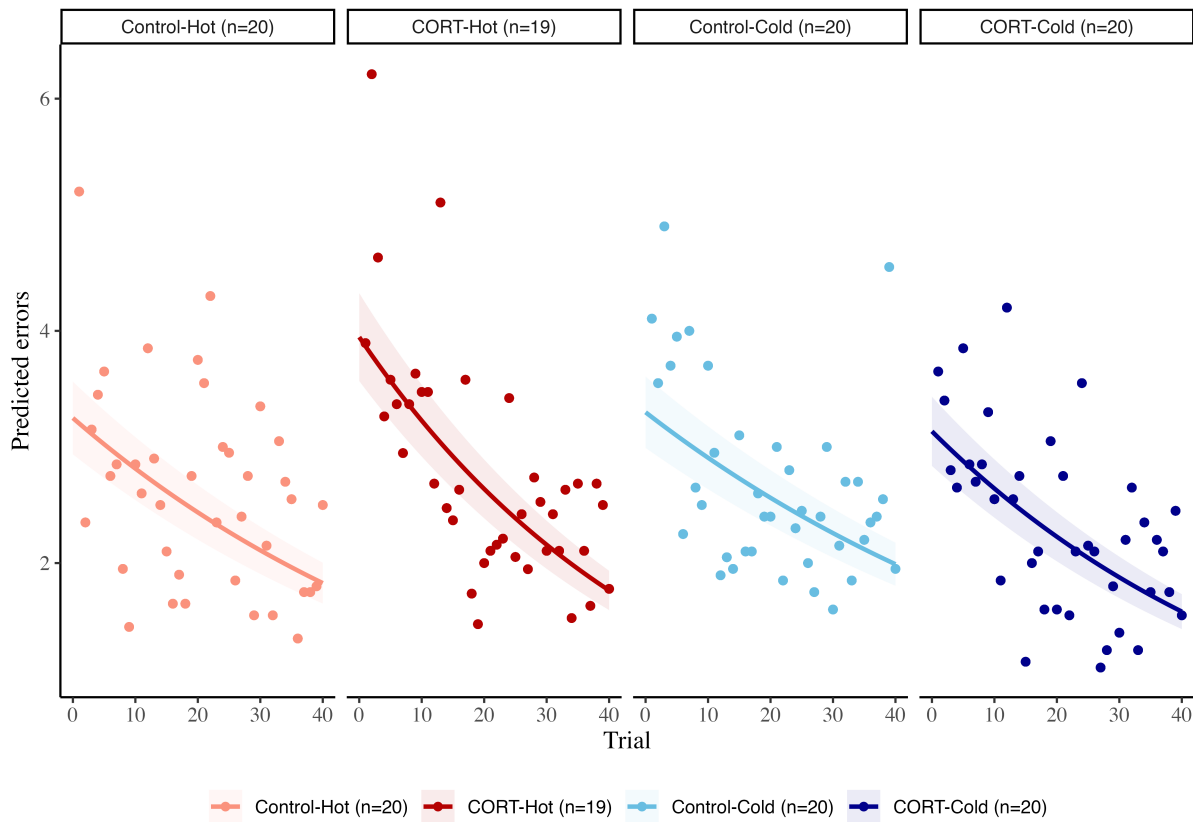
603 Data was exported from BD FACSDiva as individual *.fcs (“flow cytometry standard”) files for
604 each sample, then imported into FlowJo (v. 10.1) for processing.

605 **Data processing:** In FlowJo v. 10.1 we first transformed all fluorescent data to a logarithmic
606 base 10 scale, then applied a basic gating process across all channels by filtering to observations
607 within the detectable range (10^1 - 10^5) to remove any off-scale events. We then used a backgating
608 process wherein we aimed to identify the approximate FSC (cell size) and SSC (cell complexity)
609 range of viable cells that were positive for all stains. We primarily used the BUV-496 channel
610 (Hoechst 33342) in the backgating process to identify intact, nucleated cells ($\text{BUV-496} > 10^3$).
611 For the mitochondrial function assay, we aimed to identify populations of viable cells containing
612 mitochondria ($\text{APC} > 103$) and actively respiring (PE and PerCP-Cy5-5 $> 10^3$). For the oxidative
613 damage assay, we aimed to identify populations of cells exhibiting both DNA damage (Alexa-
614 Fluor 488 > 103) and lipid peroxidation (PerCP $> 10^3$). When backgating was done, we filtered
615 the data to the FSC by SSC range that captured the ideal population. We used the backgated
616 population for compensation of fluorescent spillover between different fluorescent probes. To
617 account for fluorescent spillover, we used a traditional compensation matrix using the
618 compensation function of FlowJo v.10.1. We identified the “positive” population for each
619 channel as the brightest ~2.5% of the distribution of observations in the respective single-color
620 control for that channel and used unstained controls as a universal negative. We visually
621 inspected the compensation matrix and its effects on population distributions for under- and
622 over-compensation, whereupon we changed the compensation matrix manually until data was
623 properly compensated. We applied the compensation matrix to all samples for downstream
624 processing. Following compensation, we again gated the data following the same process as for
625 backgating but using the compensated parameters for each channel. Following gating, we

626 exported the geometric mean (mean fluorescent intensity; MFI) and robust confidence-values for
627 each channel for each sample. For analysis, we exported summary statistics of only the area of
628 the fluorescent signal. Although we exported robust confidence values for checking repeatability
629 between replicate samples, we used the geometric means for each individual as our main
630 response variables in analyses.

631

632 *Results of the final models*



633

634 Fig. S1. Raw data of the learning task. Each point represents the mean number of errors per day.

635 The lines represent the modeled data.

636

637 *Table S1. Estimates of the learning slopes per treatment, the 95% CI, and pMCMC values testing*
638 *the hypothesis that slope is different from 0. In bold, the values that are significant at pMCMC <*
639 *0.05.*

Treatment	Estimated slope	95 CI	pMCMC
CORT-Cold	-0.017	[-0.026, -0.008]	< 0.001
CORT-Hot	-0.020	[-0.029, -0.011]	< 0.001
Control-Cold	-0.013	[-0.021, -0.004]	< 0.05
Control-Hot	-0.014	[-0.023, -0.006]	< 0.05

640

641

642 *Table S2. Estimate of the contrasts between treatments for all the variables analysed, and*
 643 *pMCMC values testing the hypothesis that contrast is different from 0. In bold, the values that*
 644 *are significant at pMCMC < 0.05.*

Variable	Predictor	Contrast	pMCMC contrast
Mit density	Temperature	-0.018	0.917
	CORT	0.134	0.471
	Interaction	0.176	0.437
Metabolic capacity	Temperature	-0.036	0.839
	CORT	0.162	0.364
	Interaction	0.135	0.559
ROS	Temperature	-0.032	0.875
	CORT	0.148	0.450
	Interaction	0.199	0.382
DNA damage	Temperature	0.007	0.970
	CORT	0.217	0.394
	Interaction	-0.128	0.706
Lipid peroxidation	Temperature	-0.601	0.106
	CORT	0.093	0.701
	Interaction	-0.037	0.909
Learning slopes	Temperature	-0.002	0.701
	CORT	0.005	0.416
	Interaction	0.001	0.881

645 Contrasts were done by:

646 - *Temperature*: $\beta_{\text{Hot}} - \beta_{\text{Cold}}$

647 - *CORT*: $\beta_{\text{CORT}} - \beta_{\text{Control}}$

648 - *Interaction*: $(\beta_{\text{Control-Hot}} - \beta_{\text{CORT-Hot}}) - (\beta_{\text{Control-Cold}} - \beta_{\text{CORT-Cold}})$

649

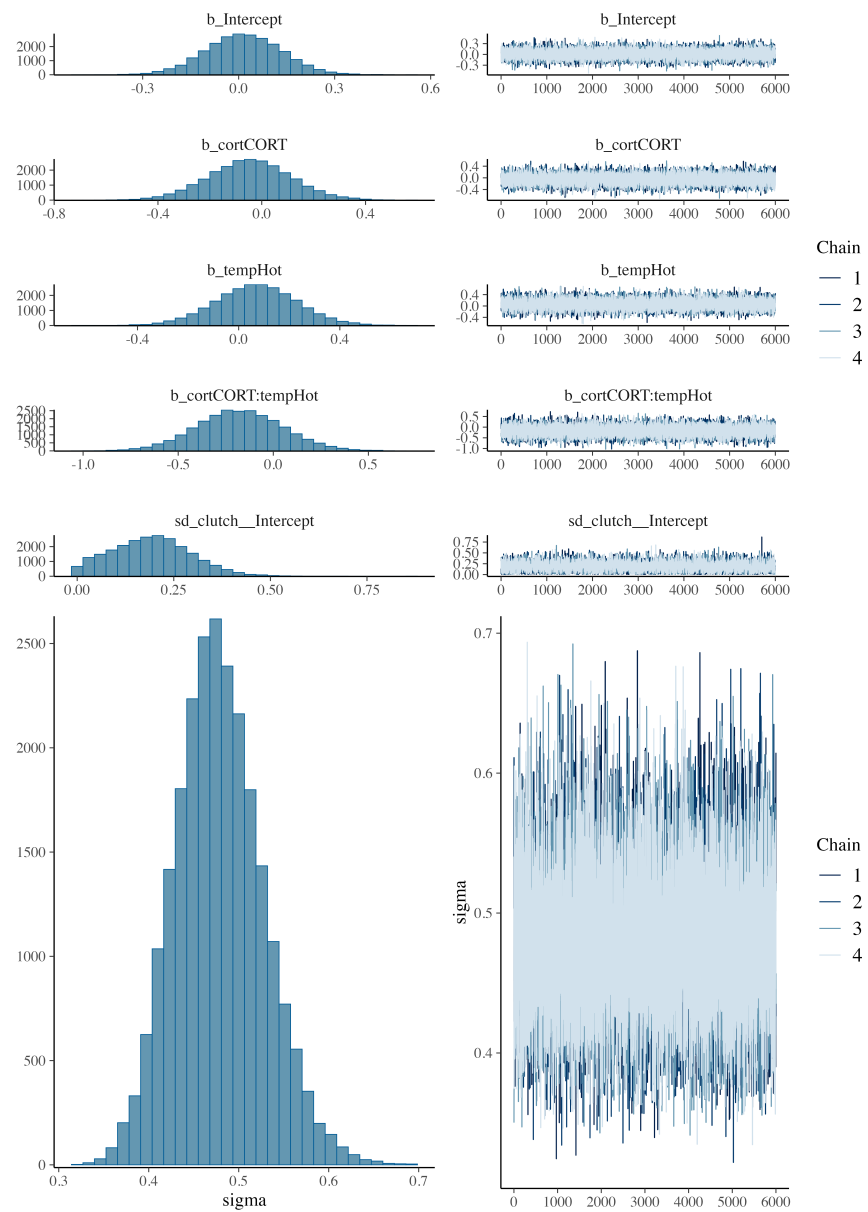
650 *Results SEM*

651 *Table S3. Estimated direct, indirect, and total coefficients from the multivariate model*

Response	Predictor	Direct effects	Indirect effects	Total effects
Learning	Mitochondrial density	0.068 [-0.270, 0.402]	0.003 [-0.036, 0.049]	0.071 [-0.269, 0.408]
	Metabolic capacity	0.025 [-0.311, 0.358]	-0.012 [-0.124, 0.088]	0.013 [-0.329, 0.357]
	ROS	-	-0.011 [-0.109, 0.080]	-0.011 [-0.109, 0.080]
	DNA damage	0.031 [-0.185, 0.241]	-	0.031 [-0.185, 0.241]
	Lipid peroxidation	-0.119 [-0.324, 0.102]	-	-0.119 [-0.324, 0.102]
DNA damage	Mitochondrial density	-	-0.037 [-0.279, 0.145]	-0.037 [-0.279, 0.145]
	Metabolic capacity	-	0.137 [-0.322, 0.654]	0.137 [-0.322, 0.654]
	ROS	0.125 [-0.292, 0.540]	-	0.125 [-0.292, 0.540]
Lipid peroxidation	Mitochondrial density	-	-0.023 [-0.243, 0.159]	-0.023 [-0.243, 0.159]
	Metabolic capacity	-	0.085 [-0.374, 0.583]	0.085 [-0.374, 0.583]
	ROS	0.076 [-0.335, 0.485]	-	0.076 [-0.335, 0.485]
ROS	Mitochondrial density	-0.282 [-0.932, 0.359]	-	-0.282 [-0.932, 0.359]
	Metabolic capacity	1.090 [0.447, 1.738]	-	1.090 [0.447, 1.738]

652

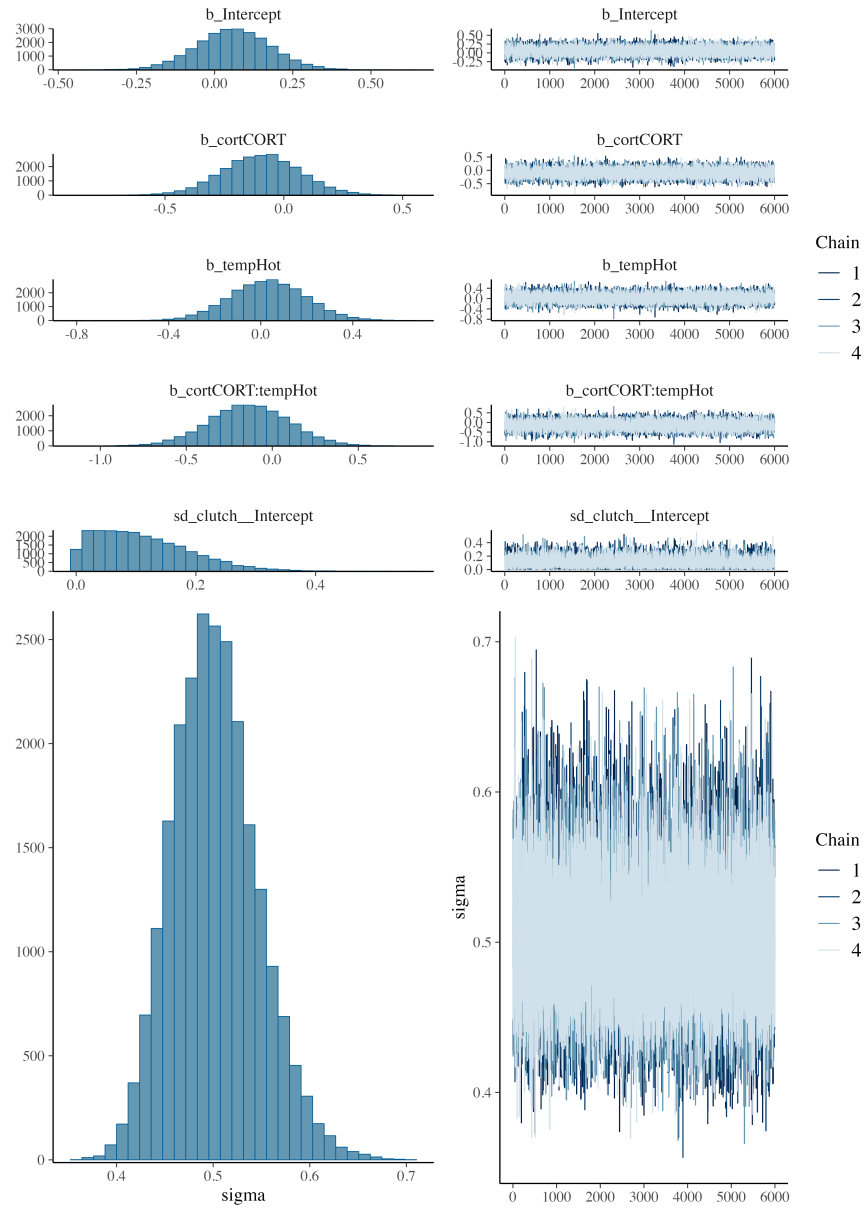
653 Final univariate models diagnostics (plots)



654 Fig. S2. Posterior predictive checks for the model of Mitochondrial Density. Formula:

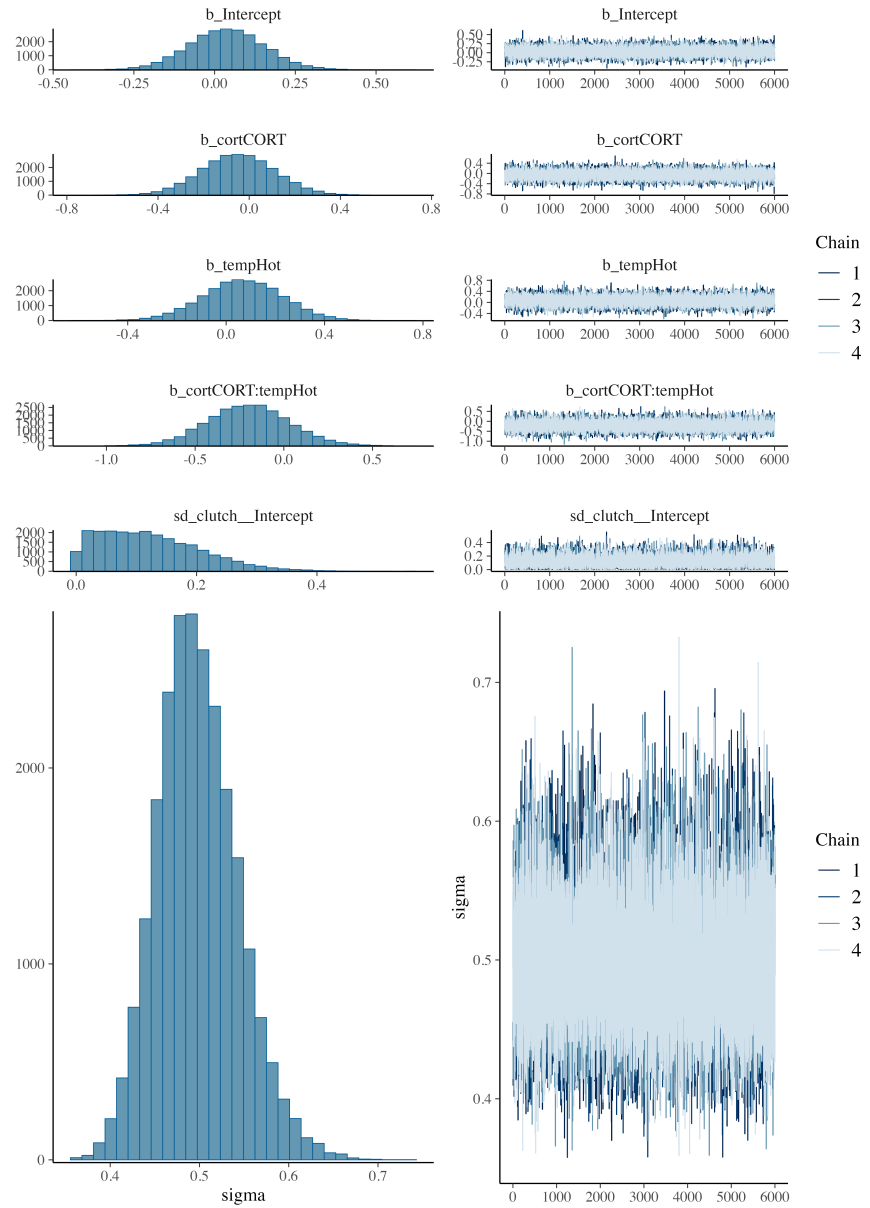
655 `mit_density ~ cort * temp + (1|clutch)`

656



657 Fig. S3. Posterior predictive checks for the model of metabolic capacity. Formula: mit_potential
 658 ~ cort * temp + (1|clutch)

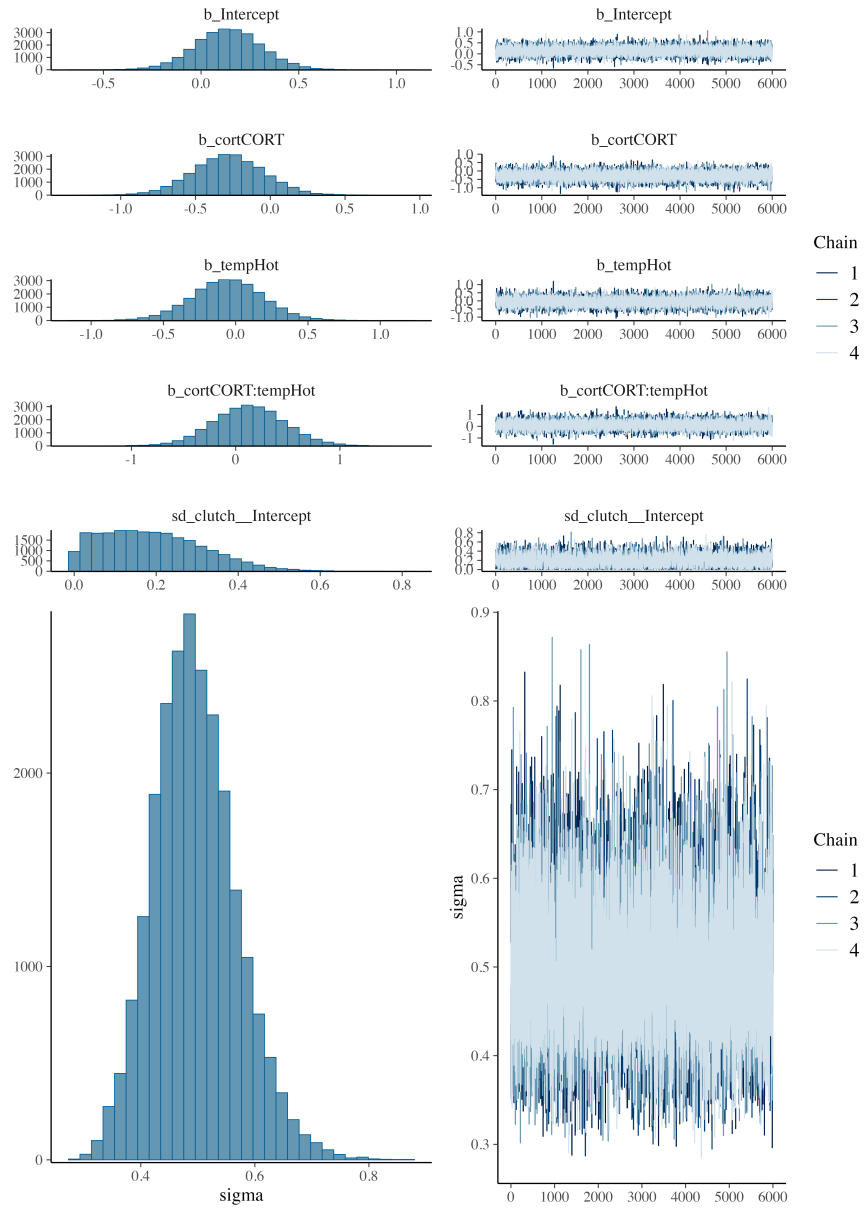
659



660 Fig. S4. Posterior predictive checks for the model of ROS. Formula: $\text{ROS} \sim \text{cort} * \text{temp} +$

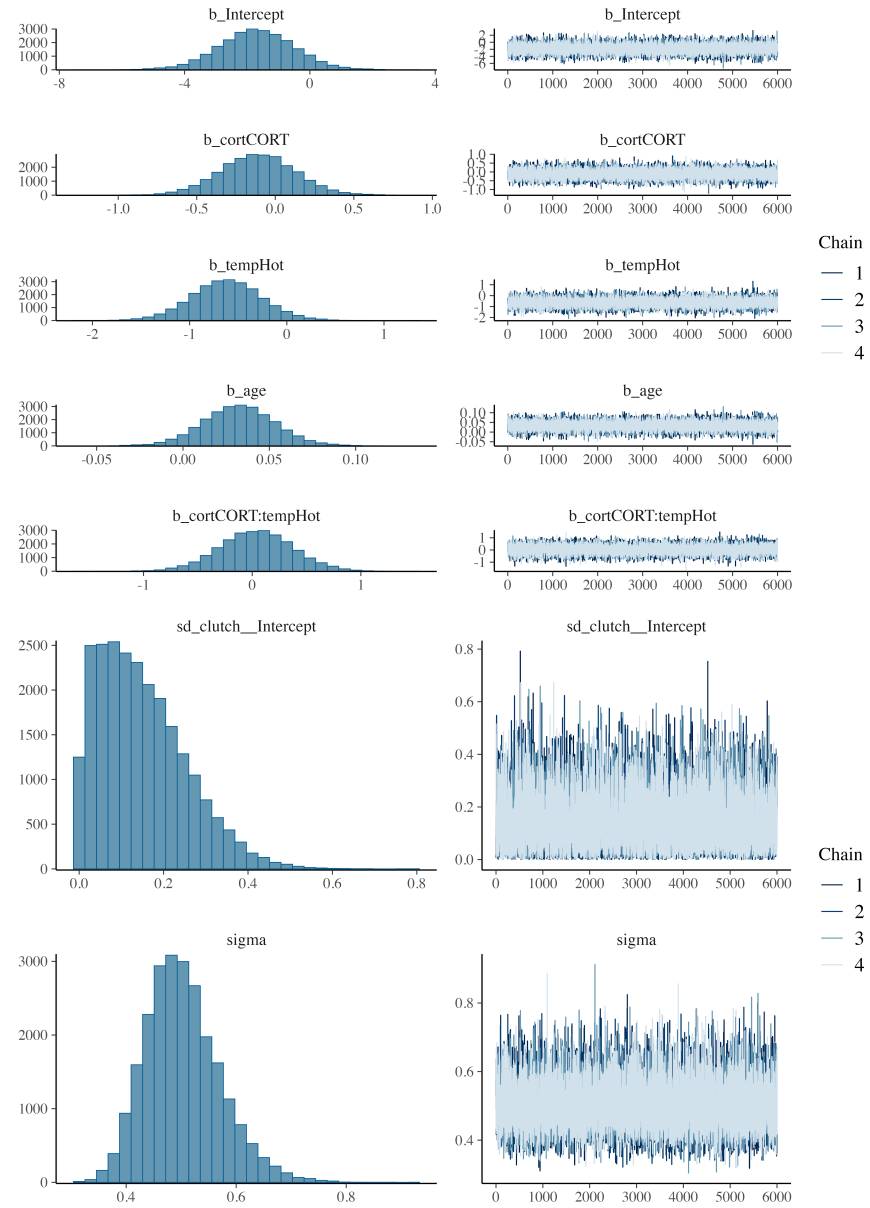
661 $(1|\text{clutch})$

662



663 Fig. S5. Posterior predictive checks for the model of DNA Damage. Formula: DNAdamage ~
 664 cort * temp + (1|clutch)

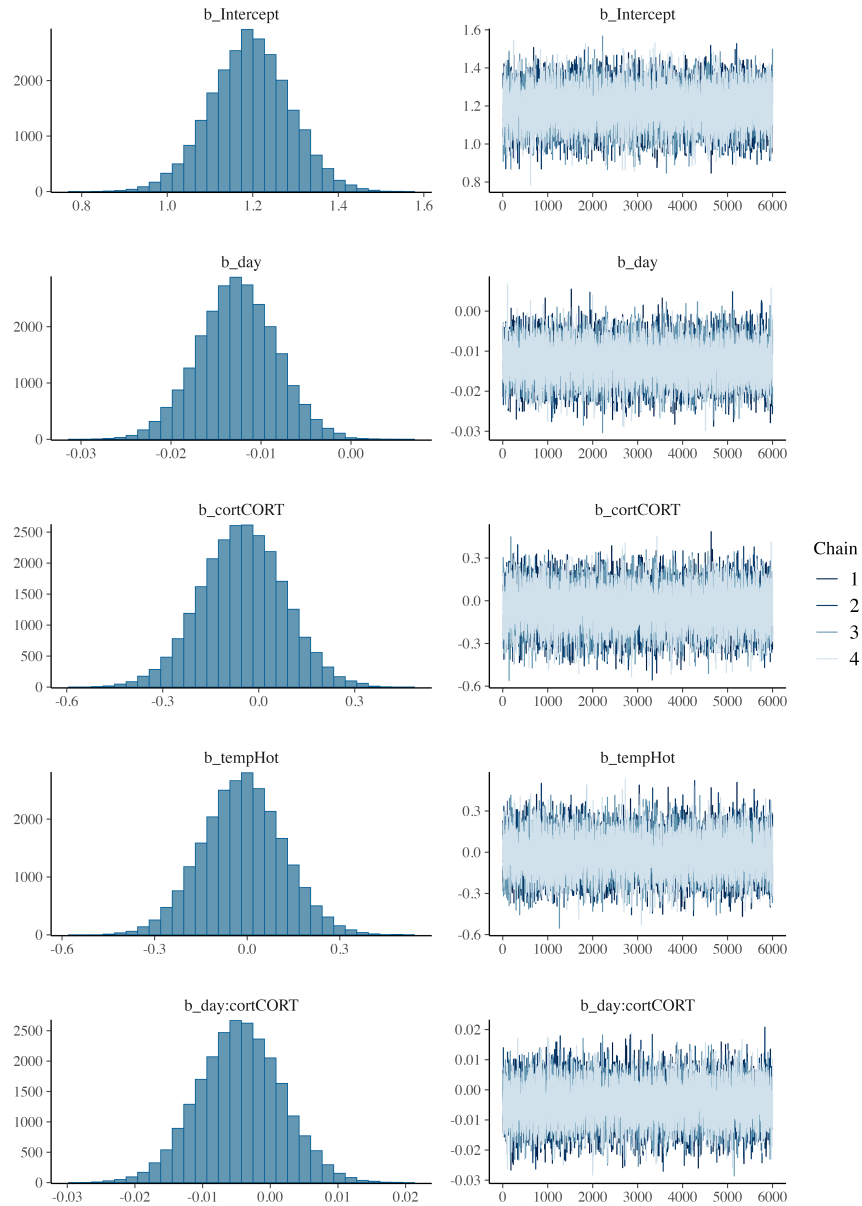
665

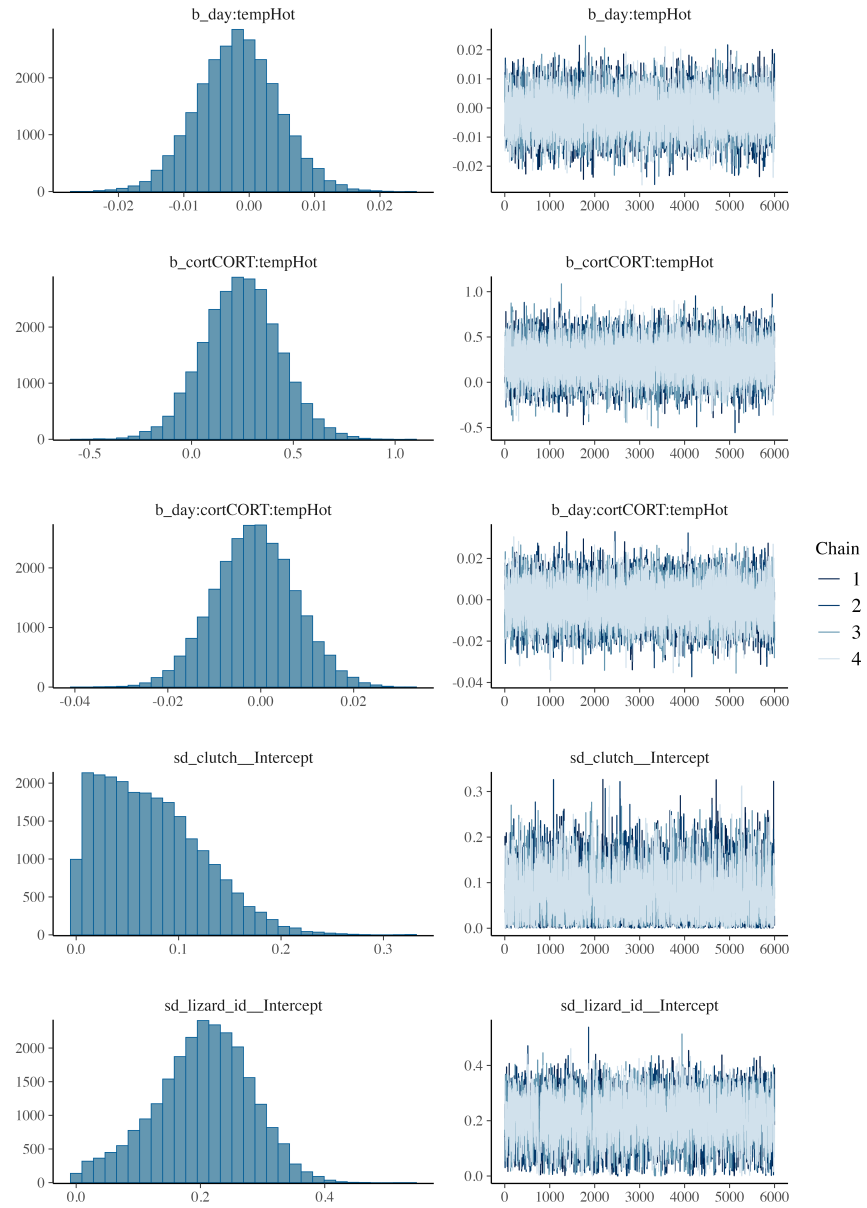


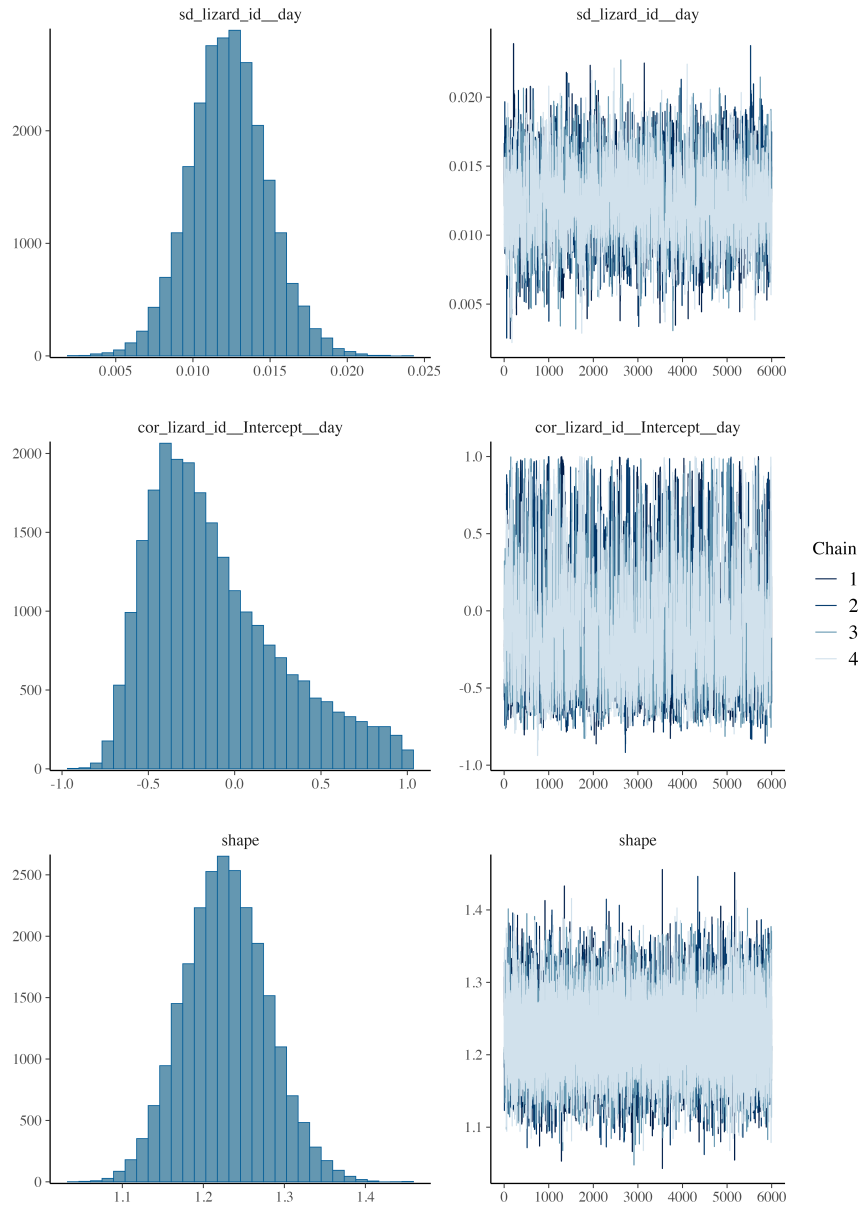
666 Fig. S6. Posterior predictive checks for the model of lipid peroxidation. Formula: peroxidation ~

667 cort * temp + (1|clutch)

668







669 Fig. S7. Posterior predictive checks for the model of spatial learning. Formula: errors ~ day *

670 cort * temp + (1 + day|lizard_id) + (1|clutch)

671

672 *Results of preliminary models*

673 *Table S4. Preliminary results of the models testing for Mitochondrial Density.*

variable	mean	median	sd	mad	q5	q95	rhat	ess_bulk	ess_tail
b_Intercept	0.470	0.460	0.866	0.855	-0.947	1.907	1	19,362.26	16,116.88
b_cortCO _{RT}	-0.054	-0.055	0.161	0.160	-0.316	0.211	1	23,841.57	18,938.53
b_tempHt	0.177	0.175	0.255	0.254	-0.240	0.598	1	18,264.83	15,601.67
b_age	-0.008	-0.008	0.015	0.015	-0.033	0.016	1	18,809.92	15,827.44
b_sexm	-0.012	-0.012	0.122	0.122	-0.212	0.187	1	32,791.21	19,114.69
b_cortCO _{RT:tempHt}	-0.163	-0.161	0.234	0.231	-0.547	0.219	1	23,053.19	18,337.06

674 Model formula: mit_density ~ cort * temp + age + sex + (1|clutch). Model convergence was

675 checked through rhat and ess_bulk values. Summary indicates no effect of sex or age, so they

676 were discarded from the final models.

677

678 Table S5. Preliminary results of the models testing for Metabolic capacity.

variable	mean	median	sd	mad	q5	q95	rhat	ess_bulk	ess_tail
b_Intercept	0.302	0.296	0.847	0.839	-1.088	1.697	1	18,682.53	16,852.64
b_cortCO _{RT}	-0.095	-0.094	0.166	0.165	-0.369	0.178	1	22,493.38	18,602.43
b_tempH _{ot}	0.092	0.091	0.248	0.247	-0.315	0.501	1	18,415.30	16,061.12
b_age	-0.004	-0.004	0.014	0.014	-0.028	0.019	1	18,669.13	16,525.89
b_sexm	0.017	0.016	0.126	0.125	-0.191	0.225	1	31,266.98	17,493.28
b_cortCO _{RT:tempH_{ot}}	-0.137	-0.137	0.242	0.240	-0.534	0.258	1	21,436.04	16,972.70

679 Model formula: mit_potential ~ cort * temp + age + sex + (1|clutch). Model convergence was
 680 checked through rhat and ess_bulk values. Summary indicates no effect of sex or age, so they
 681 were discarded from the final models.

682

683 Table S6. Preliminary results of the models testing for ROS.

variable	mean	median	sd	mad	q5	q95	rhat	ess_bulk	ess_tail
b_Intercept	0.441	0.439	0.845	0.846	-0.938	1.829	1	19,954.88	17,733.51
b_cortCO _{RT}	-0.059	-0.058	0.163	0.162	-0.329	0.206	1	21,973.58	19,467.53
b_tempH _{ot}	0.160	0.157	0.245	0.245	-0.241	0.565	1	18,615.90	16,581.43
b_age	-0.007	-0.007	0.014	0.014	-0.031	0.016	1	19,777.02	17,300.71
b_sexm	0.021	0.021	0.124	0.123	-0.183	0.224	1	33,495.85	18,274.71
b_cortCO _{RT:tempH_{ot}}	-0.183	-0.184	0.236	0.235	-0.572	0.203	1	21,404.60	18,058.25

684 Model formula: ROS ~ cort * temp + age + sex + (1|clutch). Model convergence was checked

685 through rhat and ess_bulk values. Summary indicates no effect of sex or age, so they were

686 discarded from the final models.

687

688 Table S7. Preliminary results of the models testing for DNA damage.

variable	mean	median	sd	mad	q5	q95	rhat	ess_bulk	ess_tail
b_Intercept	-0.814	-0.815	1.333	1.286	-2.975	1.384	1	14,193.24	15,015.86
b_cortCO _{RT}	-0.286	-0.287	0.249	0.244	-0.695	0.125	1	16,764.42	17,646.72
b_tempH _{ot}	-0.278	-0.280	0.402	0.393	-0.936	0.384	1	12,803.98	14,601.59
b_age	0.017	0.017	0.023	0.022	-0.021	0.054	1	13,624.26	14,032.51
b_sexm	0.030	0.031	0.185	0.181	-0.274	0.330	1	20,984.11	17,159.64
b_cortCO _{RT:tempH_{ot}}	0.108	0.107	0.355	0.350	-0.475	0.690	1	14,479.58	15,703.47

689 Model formula: DNAdamage ~ cort * temp + age + sex + (1|clutch). Model convergence was
 690 checked through rhat and ess_bulk values. Summary indicates no effect of sex or age, so they
 691 were discarded from the final models.

692

693 Table S8. Preliminary results of the models testing for lipid peroxidation.

variable	mean	median	sd	mad	q5	q95	rhat	ess_bulk	ess_tail
b_Intercept	-1.960	-1.944	1.280	1.237	-4.098	0.117	1	17,308.48	15,369.02
b_cortCO _{RT}	-0.139	-0.139	0.242	0.237	-0.537	0.256	1	17,466.19	16,492.63
b_tempH _{ot}	-0.691	-0.691	0.386	0.374	-1.328	-0.056	1	14,335.87	14,037.45
b_age	0.036	0.036	0.022	0.021	0.000	0.073	1	16,551.88	15,440.72
b_sexm	0.119	0.119	0.179	0.175	-0.171	0.414	1	23,967.02	17,240.50
b_cortCO _{RT:tempH_{ot}}	0.051	0.049	0.337	0.330	-0.508	0.603	1	18,089.57	17,414.62

694 Model formula: peroxidation ~ cort * temp + age + sex + (1|clutch). Model convergence was
 695 checked through rhat and ess_bulk values. Summary indicates no effect of sex, so it was
 696 discarded from the final models. However, we saw an effect of age and we included it in our
 697 final models.

698

699 Table S9. Preliminary results of the models testing for learning.

variable	mean	median	sd	mad	q5	q95	rhat	ess_bulk	ess_tail
b_Intercept	1.350	1.348	0.546	0.537	0.455	2.256	1	14,157.443	16,878.70
b_day	-0.013	-0.013	0.004	0.004	-0.020	-0.005	1	9,398.846	13,567.40
b_cortCOR T	-0.054	-0.052	0.134	0.136	-0.275	0.164	1	10,693.409	14,518.00
b_tempHot	0.023	0.022	0.180	0.178	-0.269	0.322	1	10,924.742	15,119.67
b_sexm	-0.005	-0.005	0.080	0.079	-0.136	0.128	1	16,727.891	17,160.45
b_age	-0.003	-0.003	0.009	0.009	-0.018	0.012	1	13,505.073	16,391.78
b_day:cortCORT	-0.004	-0.005	0.006	0.006	-0.015	0.006	1	9,216.274	12,908.06
b_day:tempHot	-0.002	-0.002	0.006	0.006	-0.012	0.008	1	9,945.670	13,744.26
b_cortCOR T:tempHot	0.242	0.241	0.194	0.194	-0.076	0.563	1	10,111.700	14,279.42
b_day:cortCORT:tempHot	0.000	0.000	0.009	0.009	-0.015	0.014	1	9,169.257	12,700.42

700 Model formula: errors ~ day * cort * temp + sex + age + (1 + day | lizard_id) + (1|clutch). Model

701 convergence was checked through rhat and ess_bulk values. Summary indicates no effect of sex

702 or age, so they were discarded from the final models.

703

704 *Brain validation*

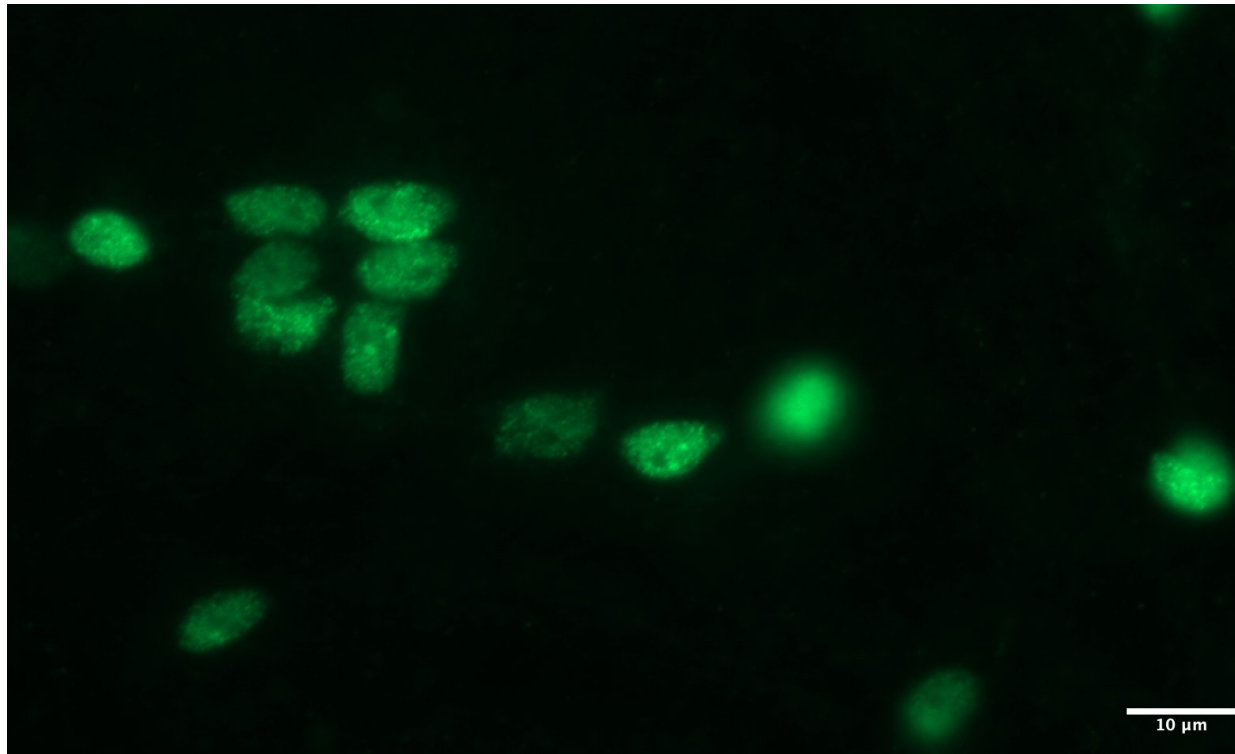
705 To ensure that neurons were not unintentionally lost during homogenization, we performed a
706 pilot study where we euthanized four lizards and prepared medial cortex homogenates using the
707 same procedures as before. However, to ensure we could identify neurons, homogenates here
708 were dyed with marker that specifically targeted neuron nuclei (Farrow et al. 2021; Storks et
709 al. 2023). We employed fluorescence microscopy and flow cytometry to check for the presence
710 of neurons in the homogenates.

711 Euthanasia and homogenization for each of brain region followed the procedures outlined above
712 (see *Methods 2: Flow cytometry*). Before staining the samples, cells were also fixed and
713 permeabilized as described previously (see *Methods 2: Flow cytometry*). Following
714 permeabilization, we centrifuged the samples at 1000 RCF for 10 minutes and resuspended the
715 pellet in 100 µL of a 1:100 dilution of NeuN + Alexa488 fluorescent conjugate to dye the
716 neuronal nuclei (Farrow et al. 2021; Storks et al. 2023). The samples were incubated at +4 °C
717 overnight.

718 The following day we centrifuged the samples at 1000 RCF for 10 minutes and resuspended the
719 pellet in 100 µL of PBS. Samples were split in two: 50 µL from each was reserved for
720 examination under a Zeiss AxioObserver Z1 microscope, while the remaining 50 µL from each
721 sample was pooled into a single tube for flow cytometry analysis. . Flow cytometry of stained
722 cells allowed us to validate that our gating strategy was correct.

723 Samples examined under the microscope showed a clear presence of neuronal nuclei in the
724 homogenates (Figure S13). Flow cytometry analysis also confirmed the presence of neuronal

725 nuclei in the homogenates, that were similar to the size of the cells employed in the experiment
726 (mean size cells experiment = 2.765; 95% CI = [2.093, 3.139], n = 80; size neurons = 3.977495).



727 Figure S8. Fluorescence microscopy image of neuron nuclei stained with NeuN-Alexa 488.
728 Images were taken on a Zeiss AxioObserver Z1, equipped with Zeiss Axiocam 506 monochrome
729 camera. A Zeiss 38HE fluorescent filter set (450-490nm Ex, 500-550nm Em.) was used in
730 conjunction with a 63x 1.4 NA.

731 REFERENCES

- 732 **Farrow, L. F., Andronicos, N. M., McDonald, P. G. and Hamlin, A. S.** (2021). Quantitative
733 determination of neuronal size and density using flow cytometry. *Journal of Neuroscience
734 Methods*, **352**, 109081.
- 735 **Storks, L., Powell, B. J. and Leal, M.** (2023). Peeking inside the lizard brain: neuron numbers
736 in Anolis and its implications for cognitive performance and vertebrate brain evolution.
737 *Integrative and Comparative Biology*, **63(1)**, 223-237.